Lecture # 2

Electron spectroscopic studies of multiferroic oxides

D. D. Sarma

Oxides that refuse to be multiferroic!

Ln_2CuTiO_6 → Same structure as $YMnO_3$

1. D. Choudhury *et al.*, Appl. Phys. Lett. 96, 162903 (2010).
2. D. Choudhury *et al.*, Phys. Rev. B 82, 134203 (2010).

Not a ferroic at all! But it has some very interesting dielectric properties ---- very high k, low loss and lowest temperature dependence known of in single phase materials so far.

Mn-doped $SrTiO_3$

Claim of a “multi-glassy” state!

Turns out to be only glassy and not “multi”!

D. Choudhury *et al*., Phys. Rev. B 84, 125124 (2011).

Photoemission and x-ray absorption of the electronic structure of multiferroic $RMnO_3$ (R=Y,Er)

J.-S. Kang et al., PRB 71, 092405 (2005)

Motivation: Basic electronic structure information:

- Valency
- Relative energy positions of various levels

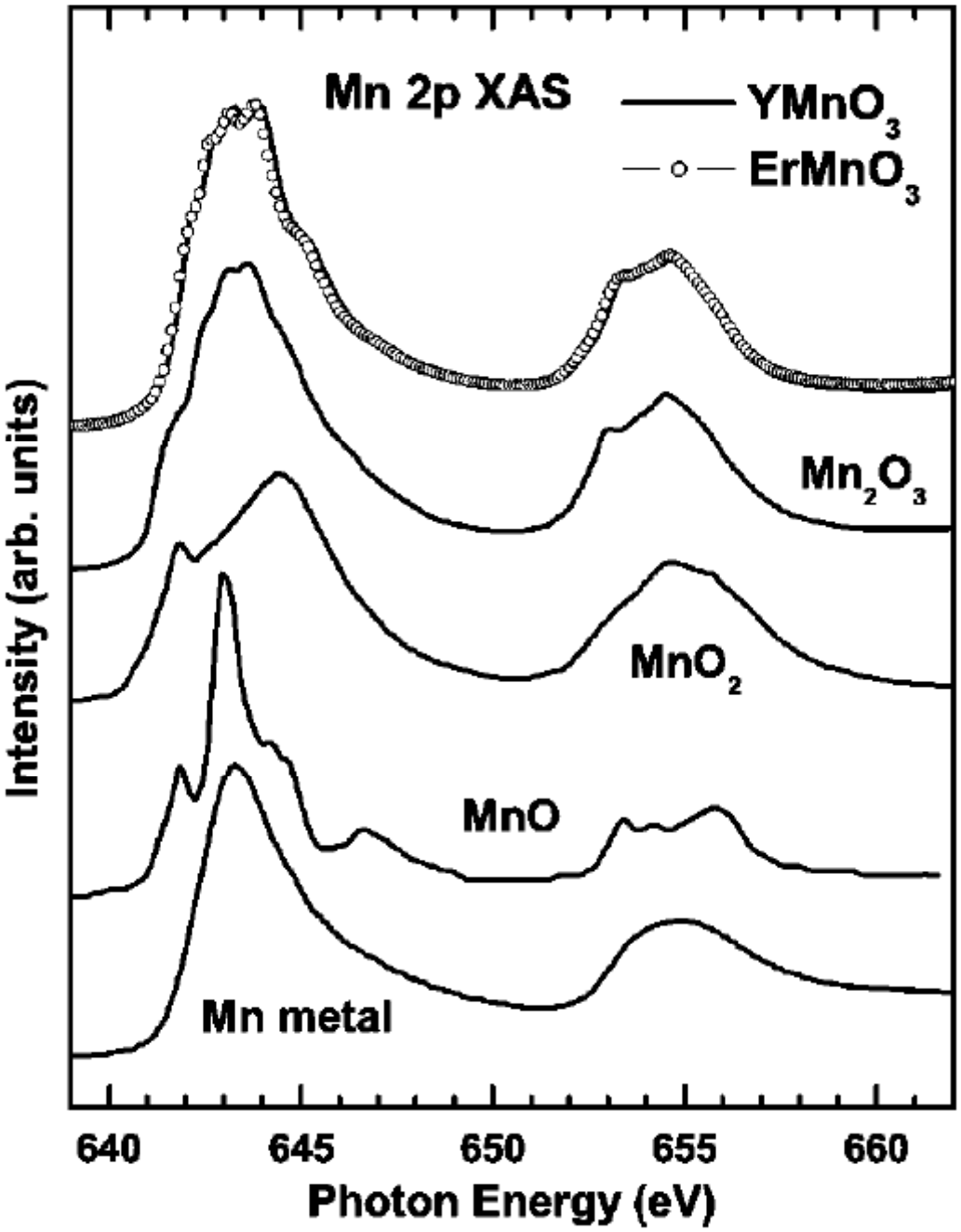

Mn^{3+}

Comparison of the Mn 2*p* XAS spectra of $YMnO_3$ (solid lines) and $ErMnO_3$ (symbols) to those of Mn_2O_3 (Mn^{3+}), MnO_2 (Mn^{3+}), MnO (Mn^{2+}), and Mn metal.

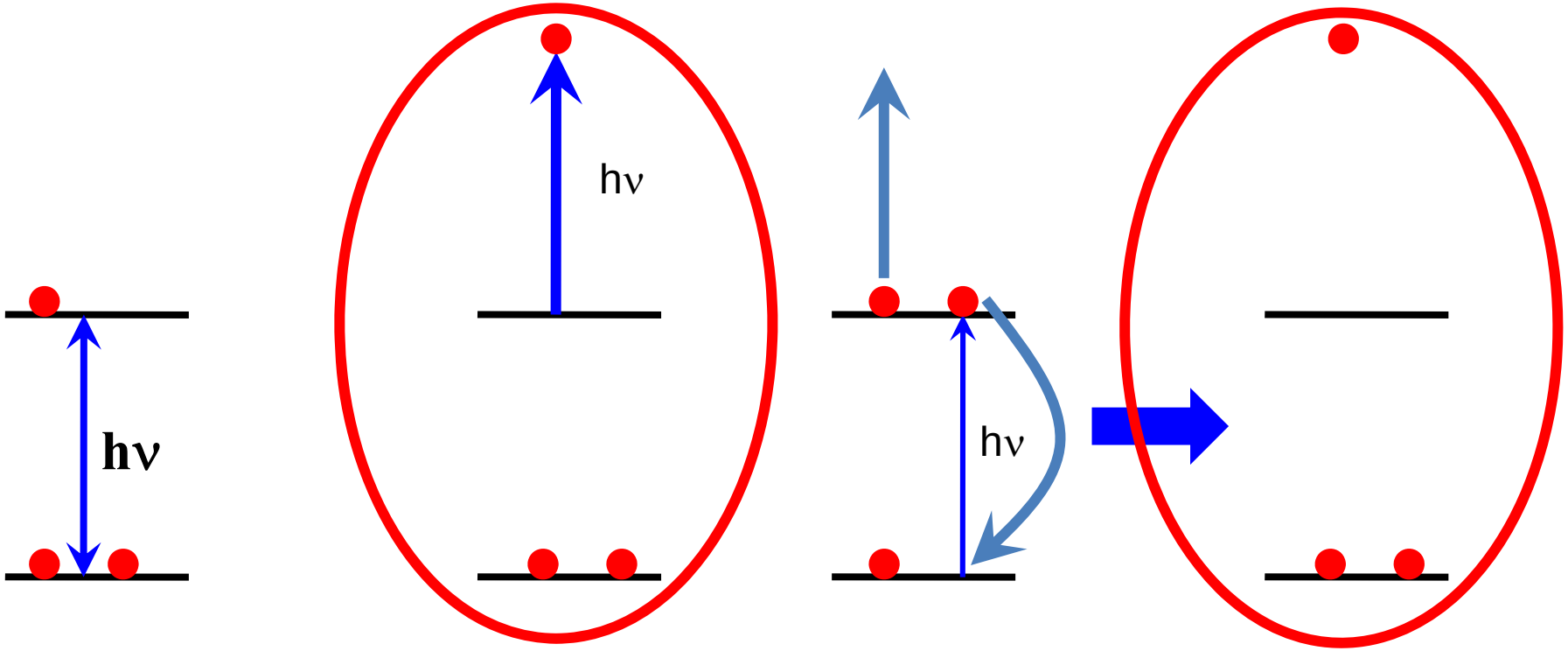

(1) Photoemission **(2) Photoabsorption followed by autoionization**

Identical final states via two different paths

Interference between these two paths leading to strong variation in the photoemission cross-section with hν.

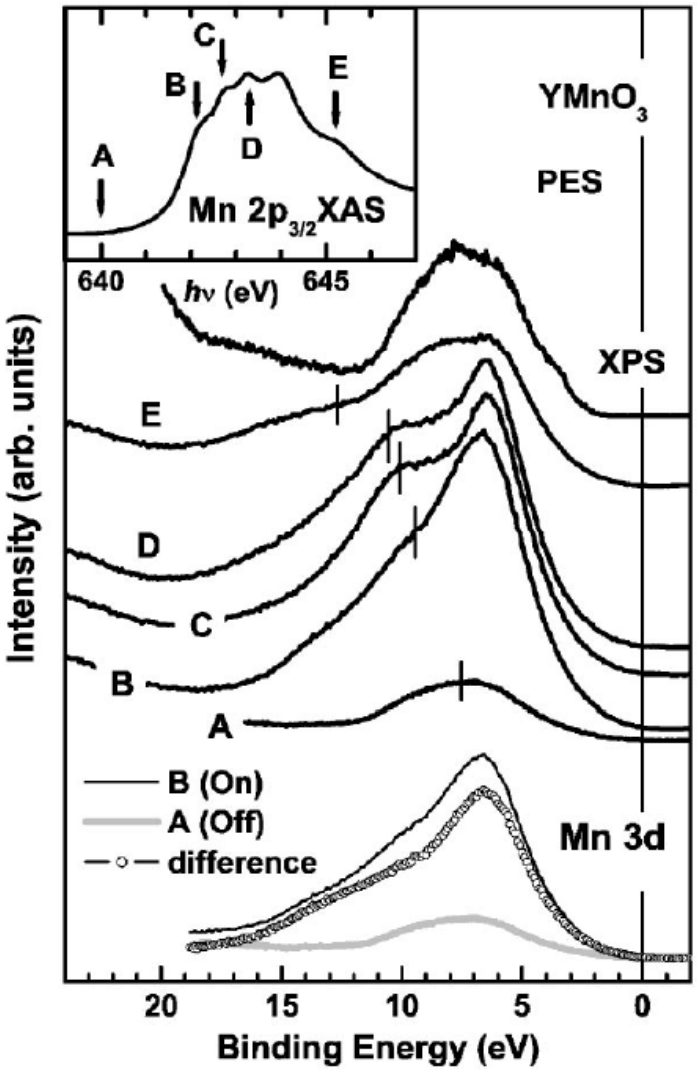

Valence-band PES spectra of $YMnO_3$ near the Mn $2p_{3/2}$ → 3d absorption edge.
Bottom: Comparison of the on-resonance (solid line) and off-resonance valence-band PES spectra (gray line) in Mn 2p→3d RPES, and the difference between these two (open dots).

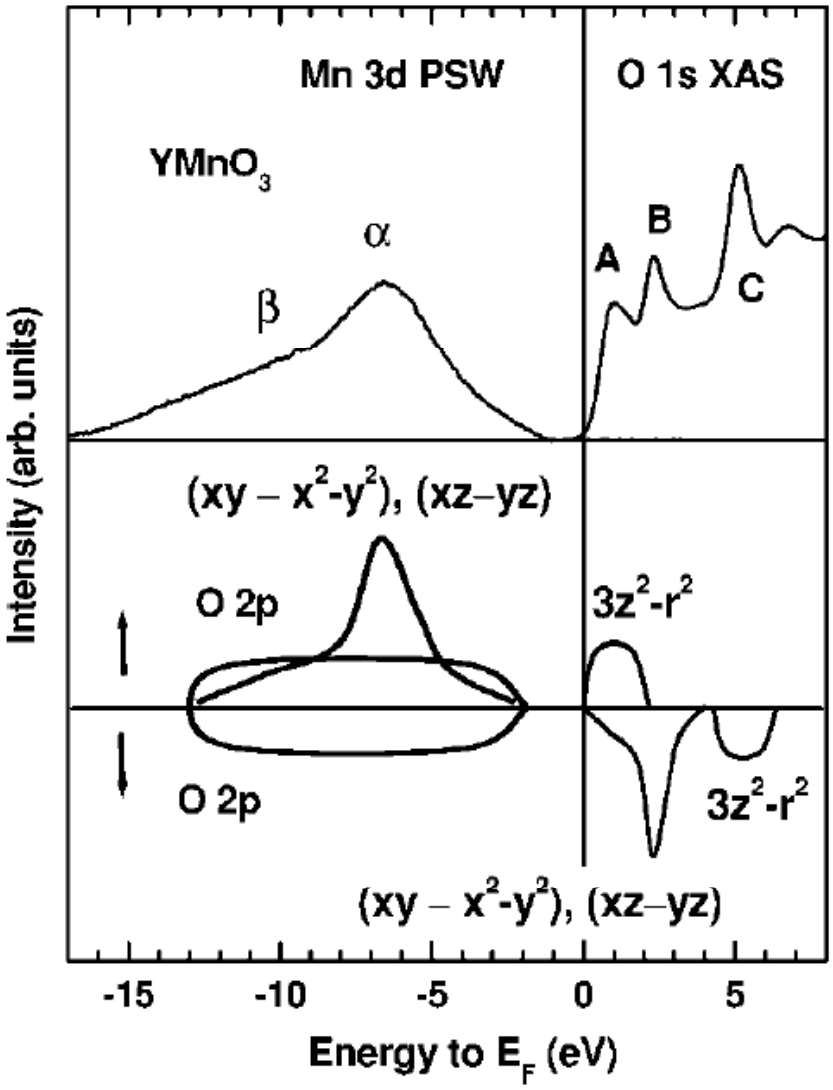

Top: Combined Mn 3*d PSW and O 1s XAS for $YMnO_3$.*
Bottom: The schematic diagram for the Mn 3*d PDOS of $YMnO_3$.*

Co–O–O–Co superexchange pathways enhanced by small charge-transfer energy in multiferroic BiCoO3

T. Sudayama et al., PRB 83, 235105 (2011)

Motivation:

- Spin state of Co^{3+}
- Why is it not a G-type antiferromagnet and not a C-type?

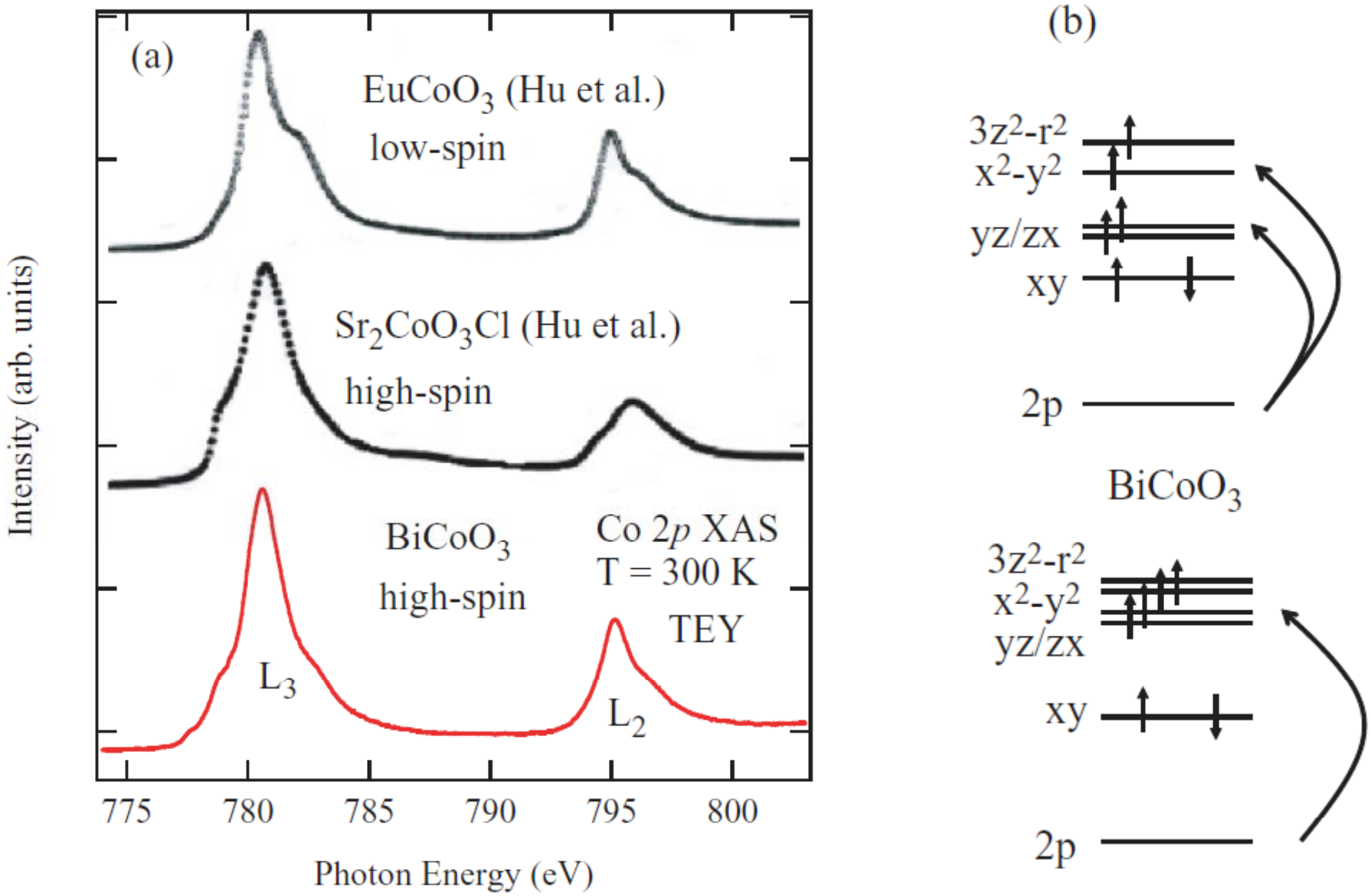

(a) Co 2p XAS spectrum of $BiCoO_3$ compared with the reference spectra of Sr_2CoO_3Cl (high-spin configuration) and $EuCoO_3$ (low-spin configuration) (Ref. 19).

(b) Electronic configurations for Sr_2CoO_3Cl (top) and $BiCoO_3$ (bottom).

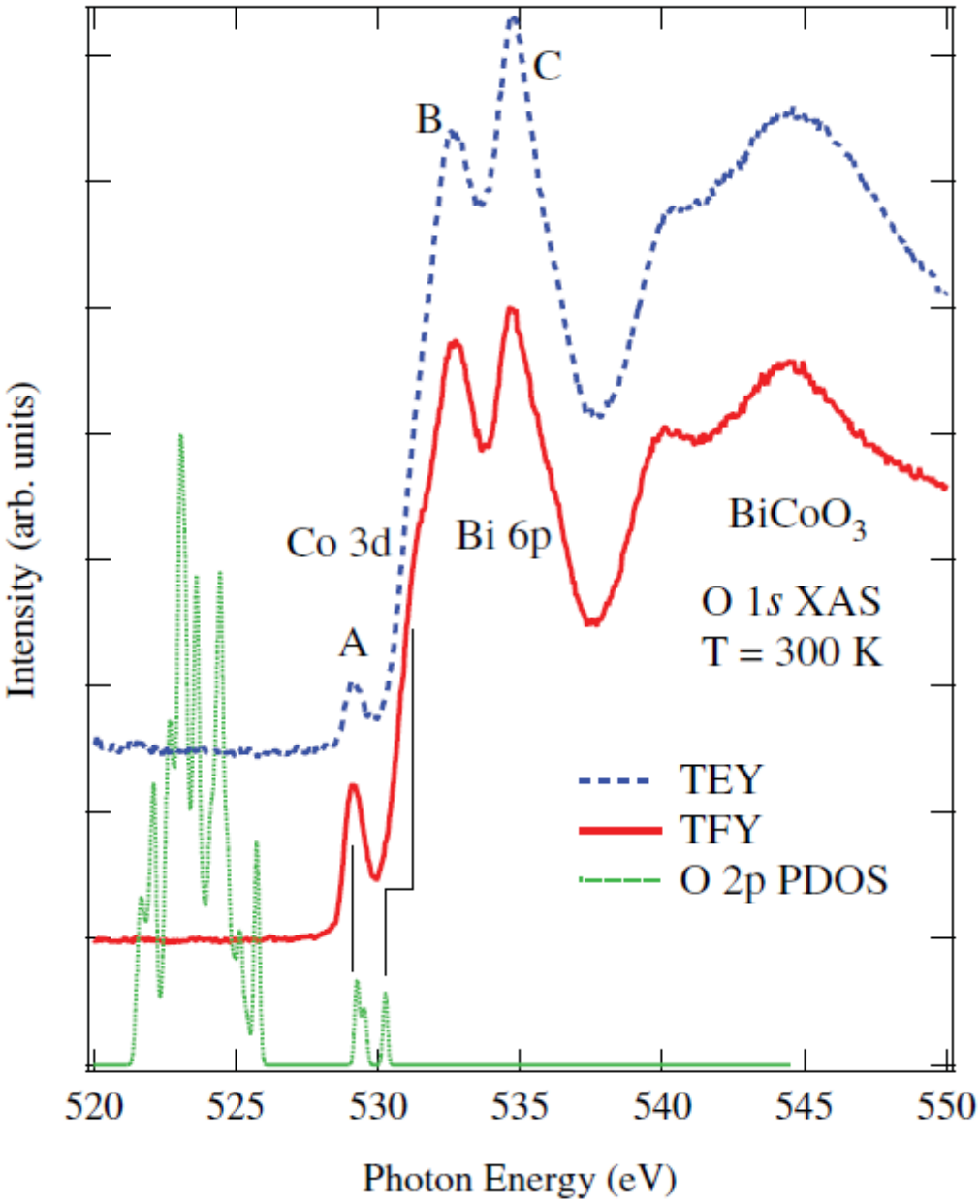

O 1s XAS spectrum of $BiCoO_3$ using TFY and TEY modes. The experimental result is compared with the O 2p partial density of states (PDOS).

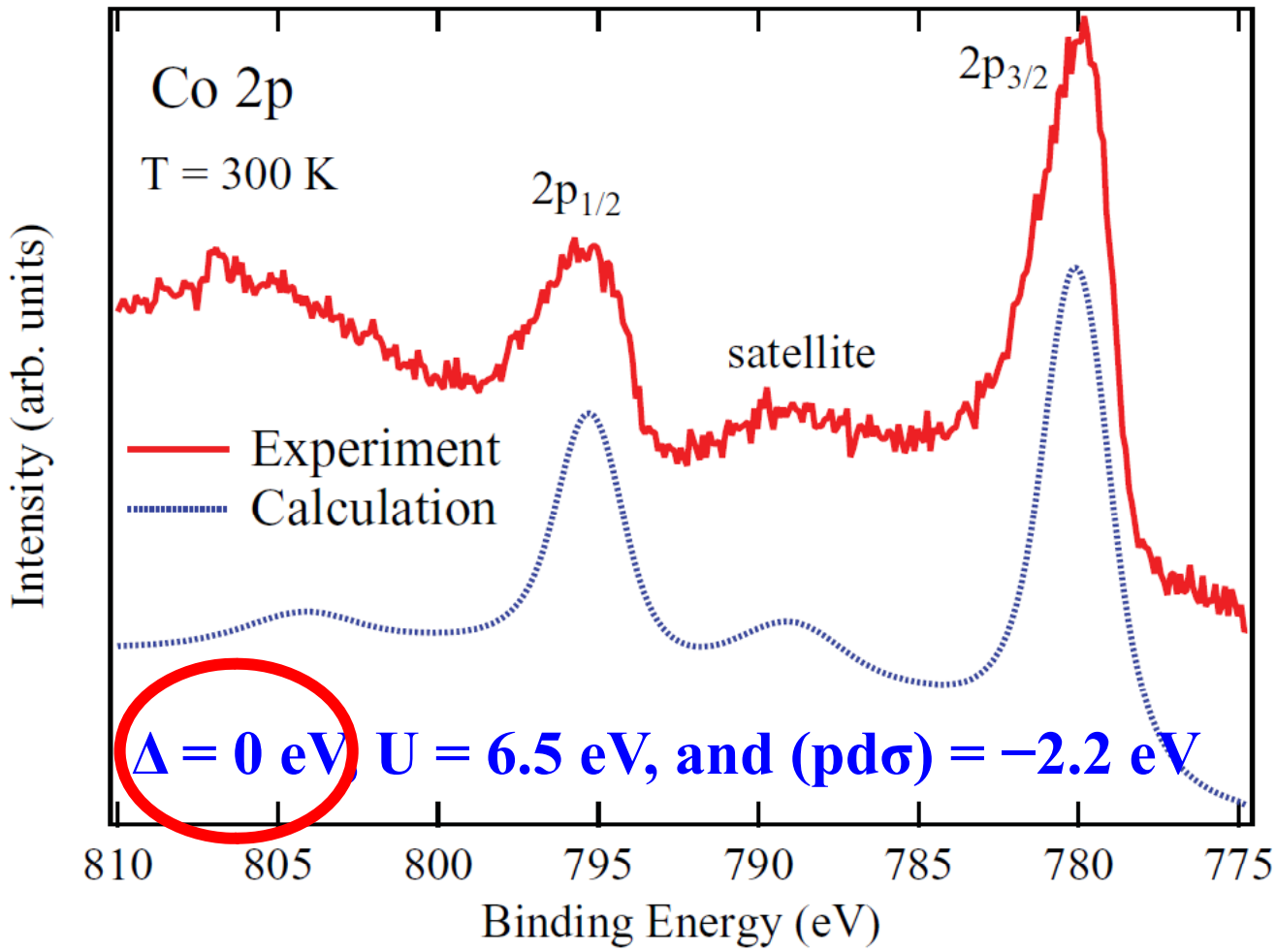

Very small charge-transfer energy, implying it does not cost much energy to excite an electron from O 2p to Co 3d.

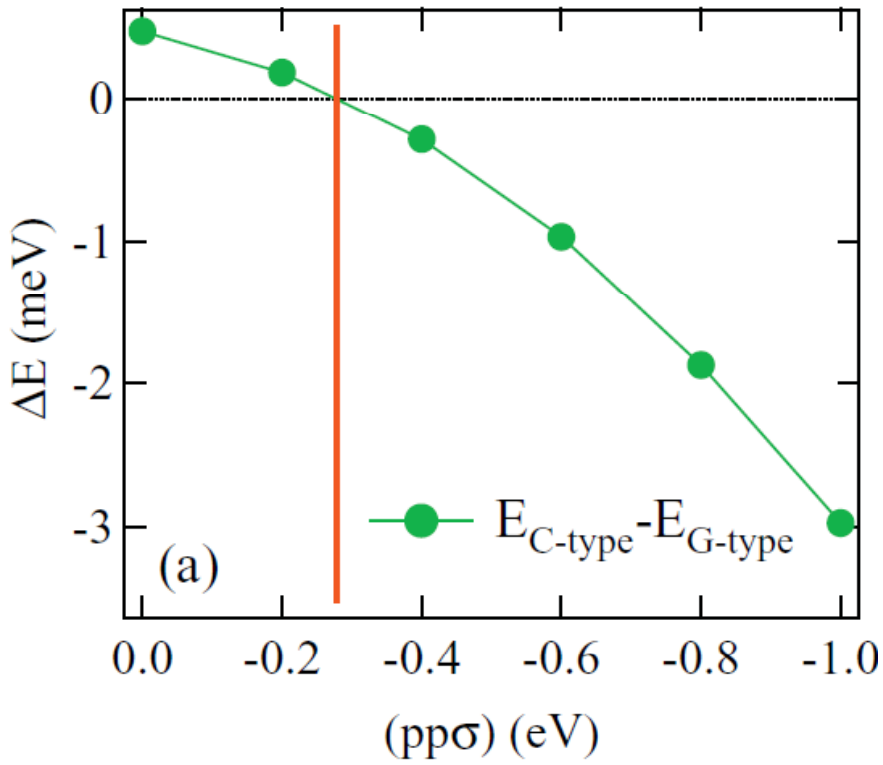

(a) A schematic drawing for crystal structure and superexchange pathways for $BiCoO_3$.

(b) C-type and G-type antiferromagnetic arrangements of Co spins.

Ferroelectricity Driven by Y d^0-ness with Rehybridization in $YMnO_3$

D.-Y. Cho et al., PRL 98, 217601 (2007)

Motivation: Is there any effect of hybridization on Y 4d?

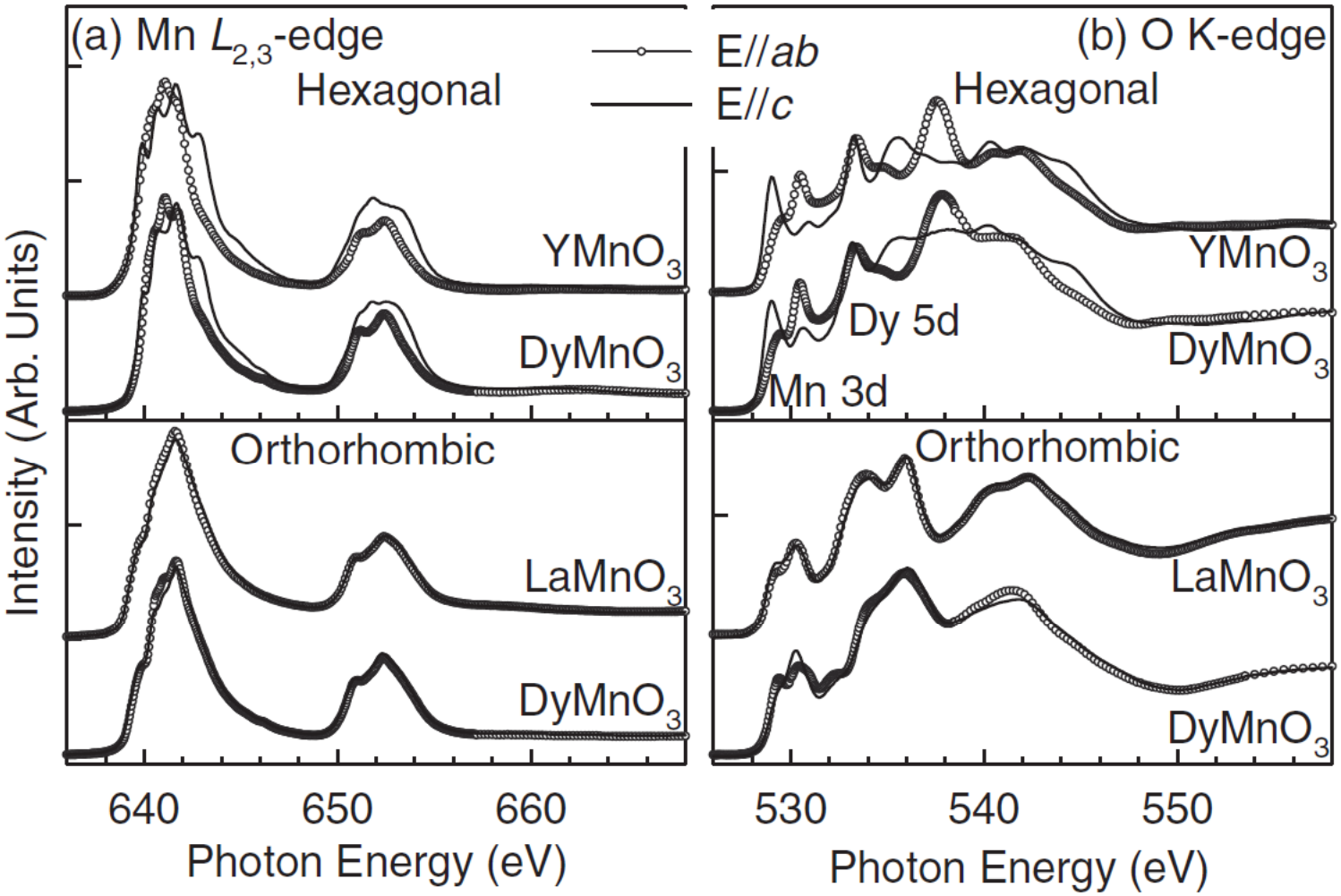

Polarization dependent XAS spectra of hexagonal $RMnO_3$ (R = Y, Dy) and orthorhombic $RMnO_3$ (R = La, Dy) at (a) Mn $L_{2,3}$- and (b) O K edge. The E ∥ c spectra for $DyMnO_3$ films were approximated by the spectra at ∠ (E,c) = 20°.

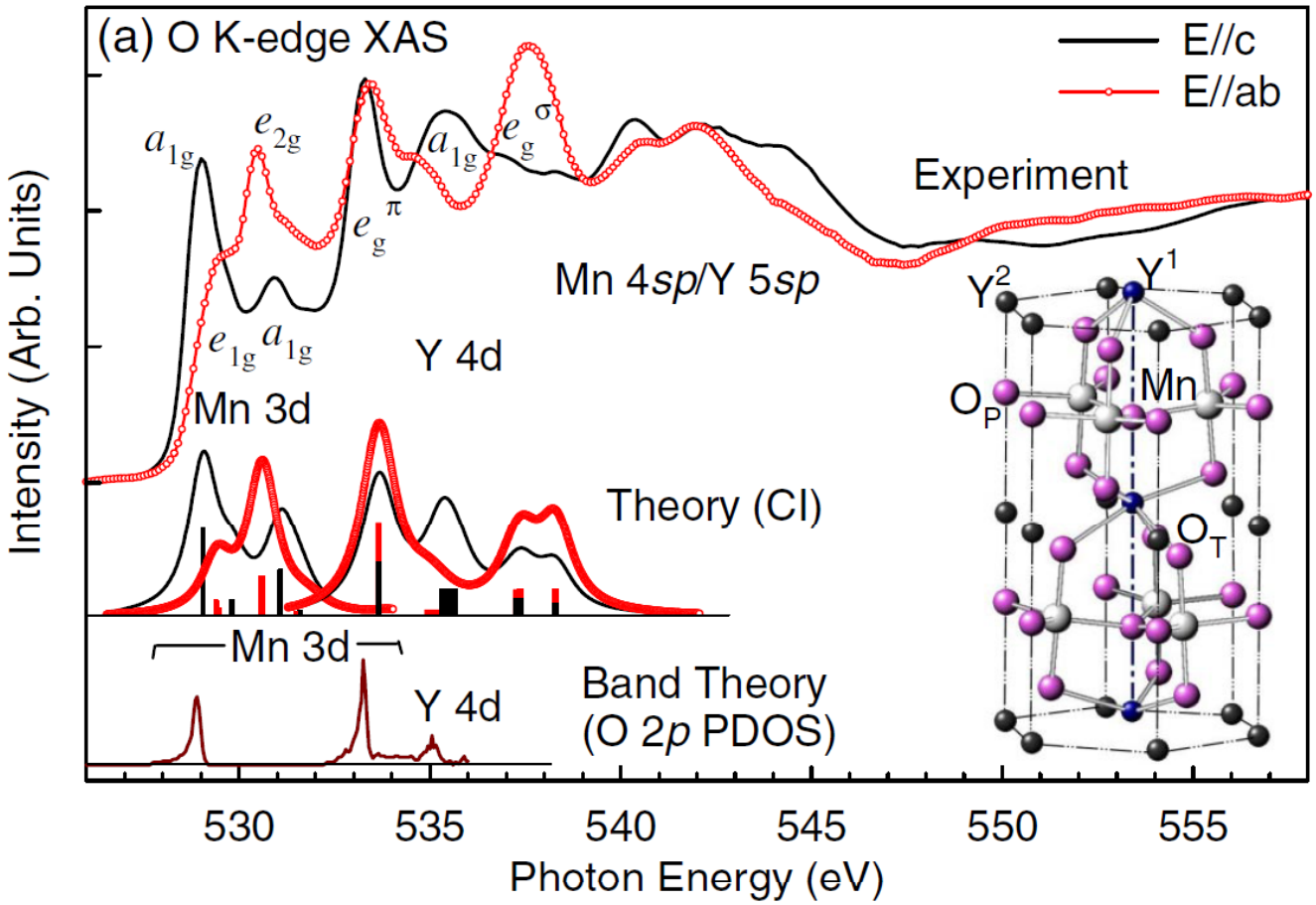

(a) O K edge polarization dependent XAS spectra of hexagonal $YMnO_3$ in comparison with the CI model calculations and the band calculations for O 2p PDOS.

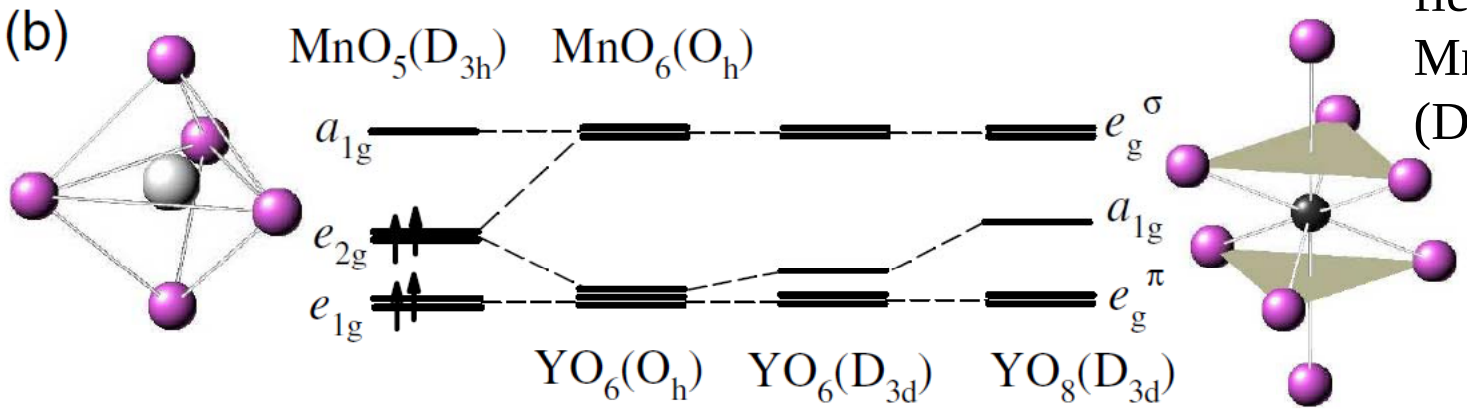

(b) Schematic crystal field splittings for MnO_5 (D3h) and YO_8 (D3d).

Electronic Origin of Giant Magnetic Anisotropy in Multiferroic $LuFe_2O_4$

K.-T. Ko et al., PRL 103, 207202 (2009)

Motivation:

- Fe^{2+} and Fe^{3+} with a $T_{CO} \sim 320$ K and $T_C \sim 240$ K.

- Ground state is antiferroelectric, but ferroelectric state can be stabilized by cooling in presence of an electric field.

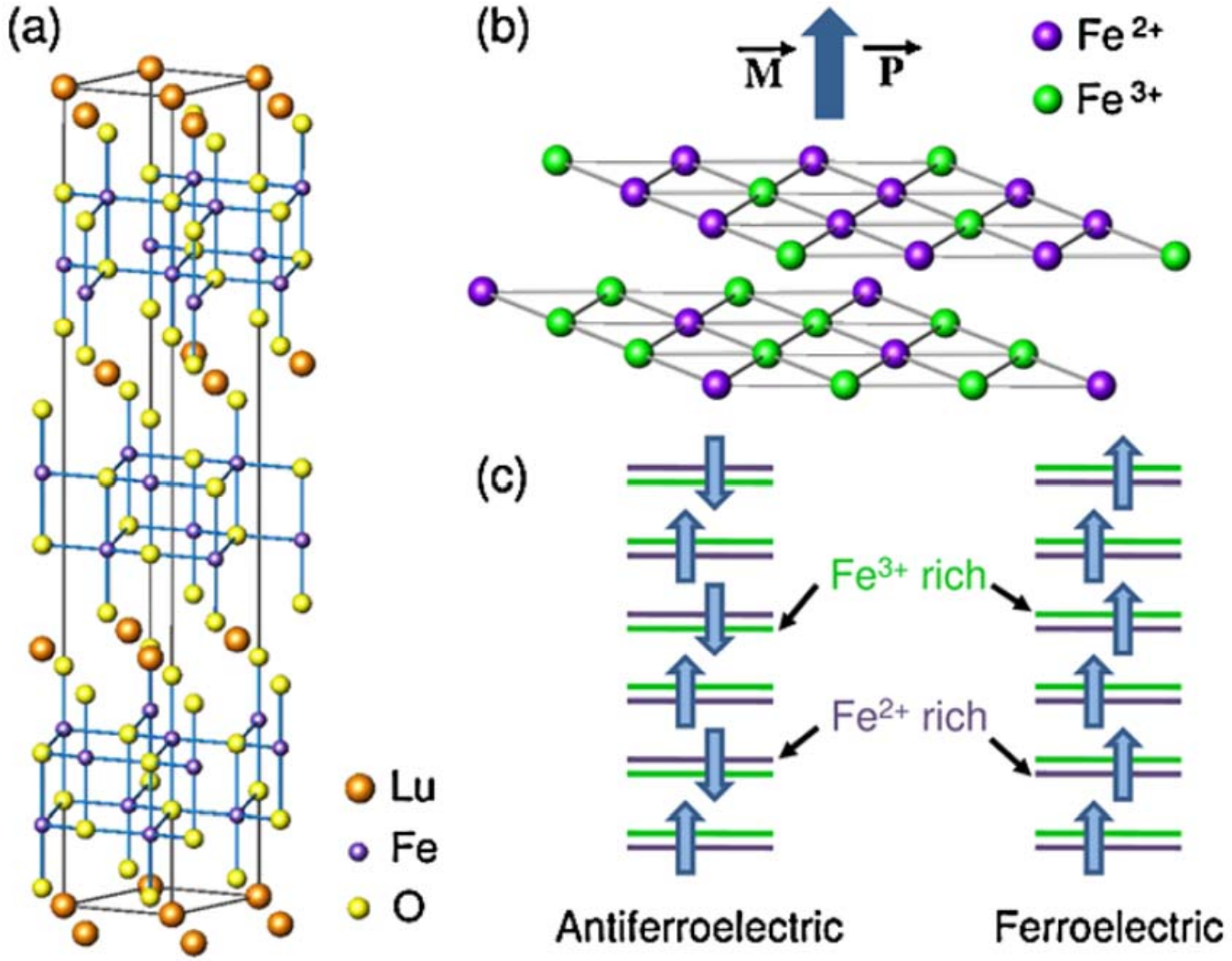

(a) Crystal structure of $LuFe_2O_4$ with Fe double layers and Lu layers.

(b) Fe^{2+} rich (2:1 Fe^{2+}=Fe^{3+} ratio) and Fe^{3+} rich (2:1 Fe^{3+}=Fe^{2+} ratio) double layer with the charge order. The electric polarization (320 K) and the magnetization (240 K) are parallel to the c axis.

(c) Schematic diagrams of two different charge orders.

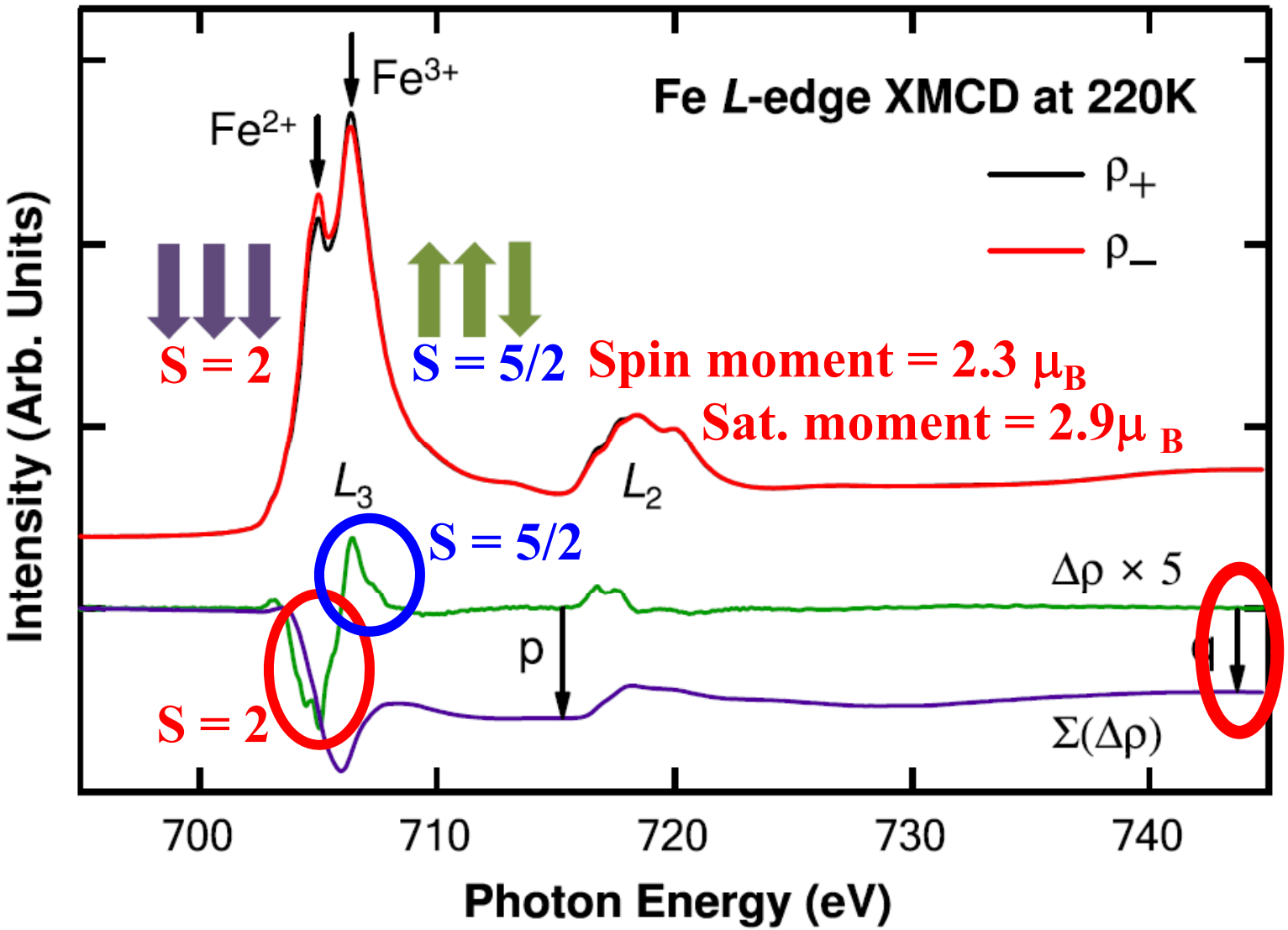

Large orbital magnetic moment (~ 0.8 μ_B) in spite of the expected quenching.

Fe $L_{2,3}$-edge XMCD spectra of $LuFe_2O_4$ at 220 K. Fe^{2+} and Fe^{3+} white lines in the L_3 region are indicated by arrows. The dichroism spectrum, $\Delta\rho = \rho_+ - \rho_-$, is obtained from the difference of the absorption spectra. The bold arrows represent the ferrimagnetic spin configuration in the tripled unit cell.

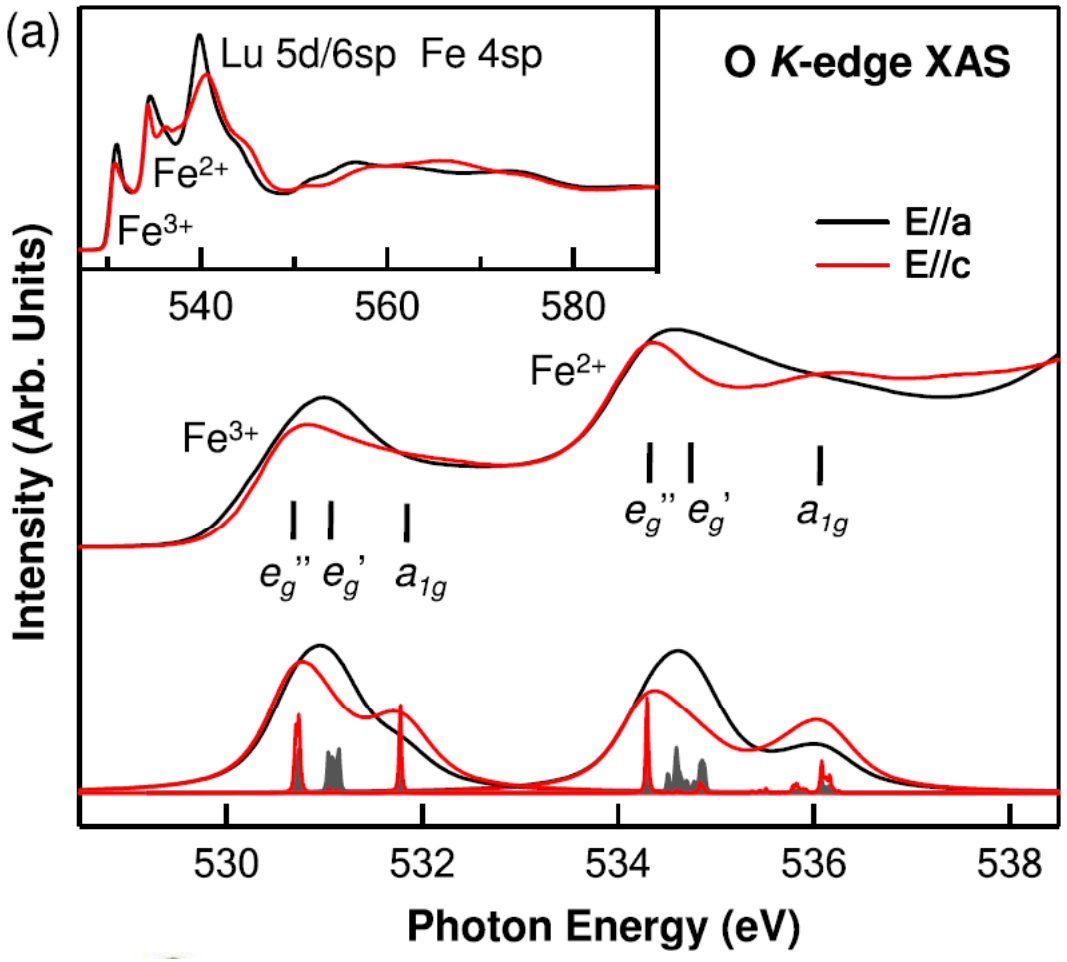

(a) Polarization dependent O K-edge XAS spectra (top) of $LuFe_2O_4$ at 250 K are compared with the CI calculation results (bottom). The wide range spectra are presented in the inset. The e'_g, e''_g, and a_{1g} orbital states under the FeO_5 crystal field are identified. (b) Schematic crystal field splitting. The lowest e''_g (d_{zx}=d_{yz}) doublet is split into m_l = +1 and -1 states by the spin-orbit coupling.

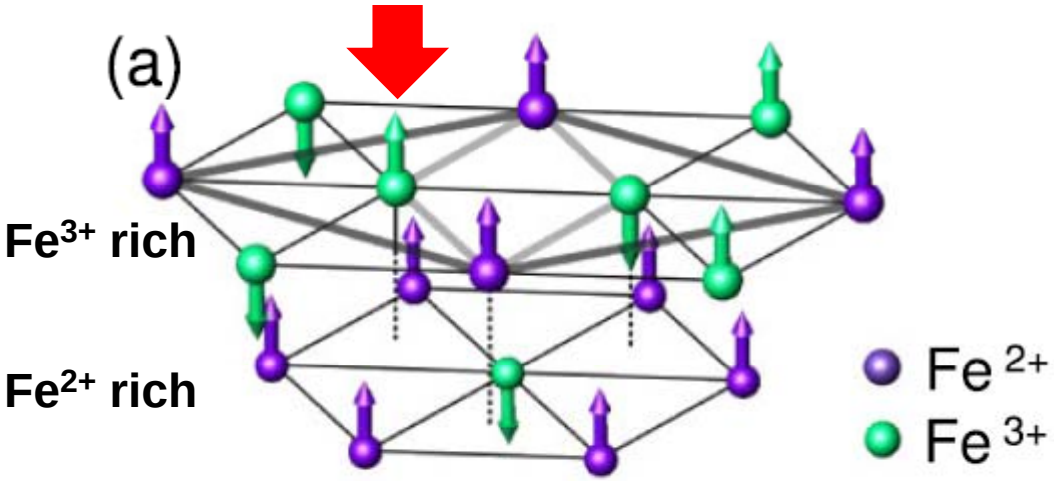
(a)
Fe3+ rich
Fe2+ rich
Fe 2+
Fe 3+

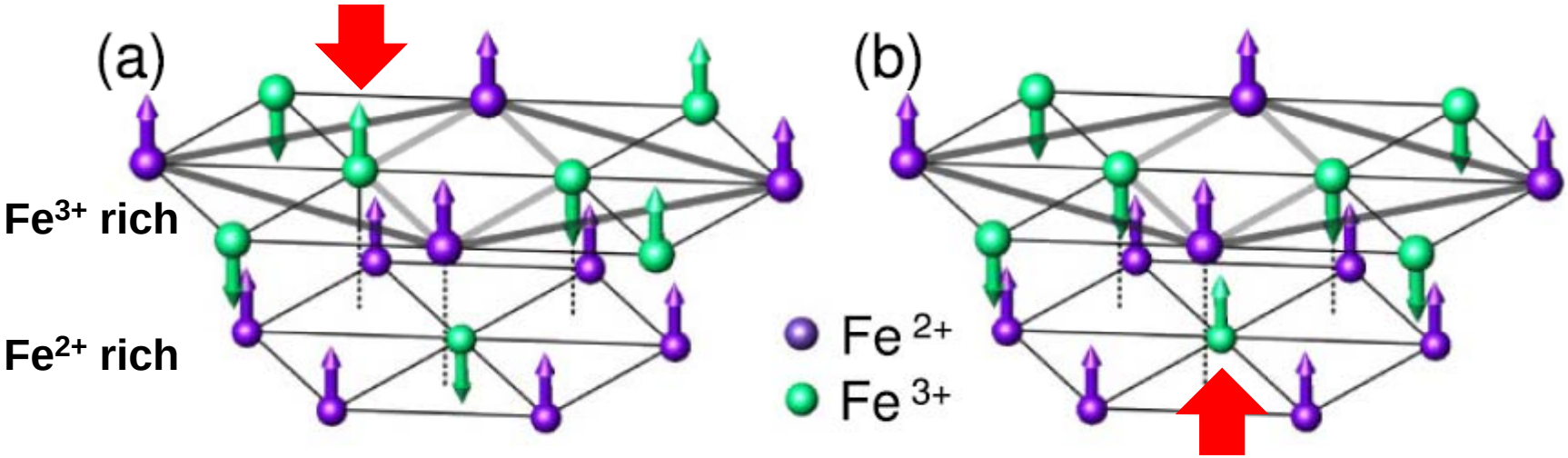
(a)
(b)
Fe3+ rich
Fe2+ rich
Fe 2+
Fe 3+

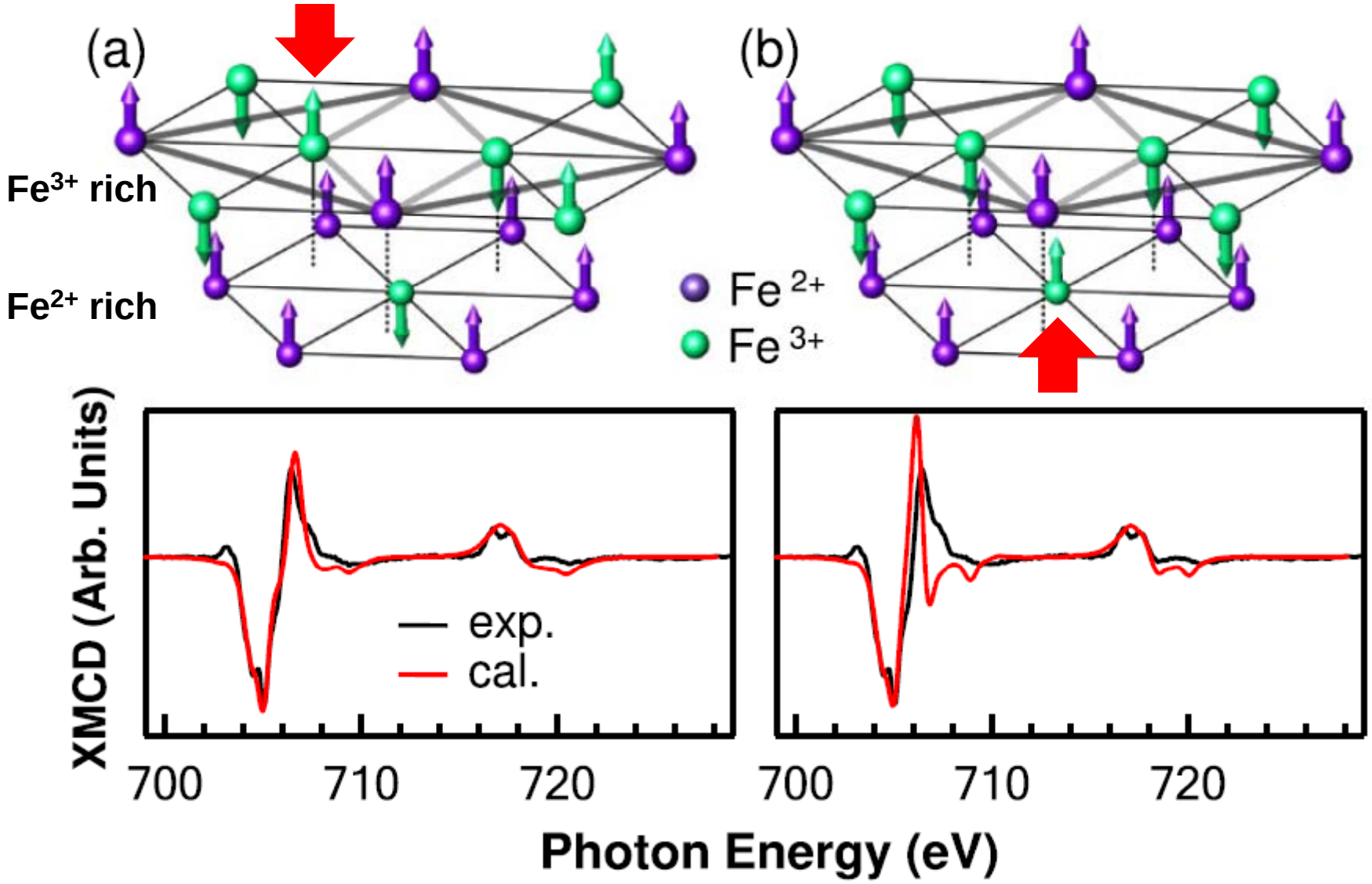

CI calculations for the XMCD spectra for the two spin structure, in which the √3 X √3 magnetic unit cell is indicated with solid thick lines; (a) antiparallel and (b) parallel Fe^{3+} spin configurations in Fe^{3+} rich layer.

Origin of ferroelectric polarization in spiral magnetic structure of $MnWO_4$

K. V. Shanavas et al., PRB 81, 212406 2010

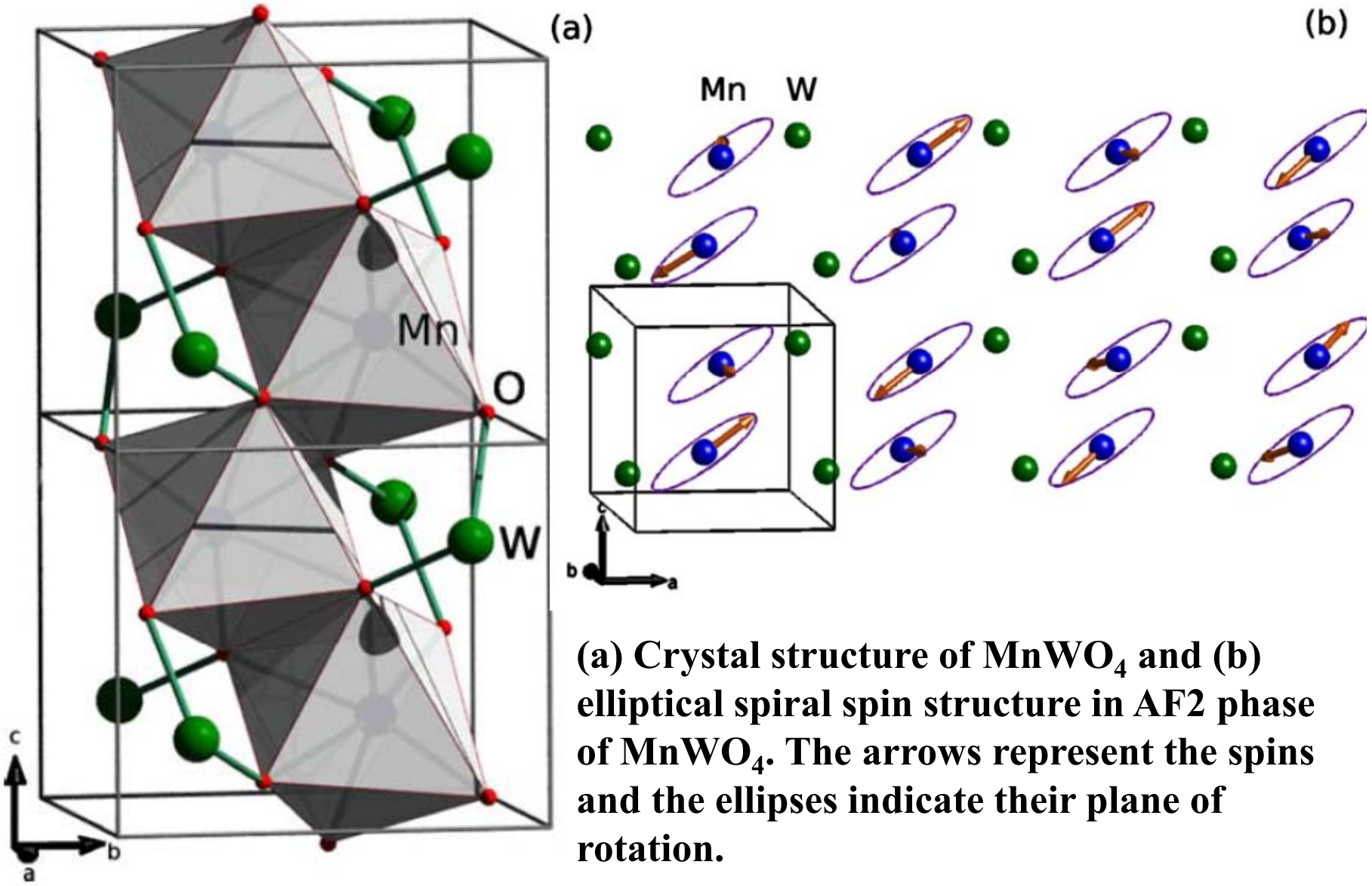

(a) Crystal structure of $MnWO_4$ and (b) elliptical spiral spin structure in AF2 phase of $MnWO_4$. The arrows represent the spins and the ellipses indicate their plane of rotation.

Ab initio calculations show that the ferroelectric polarization is critically dependent on spin-orbit coupling.

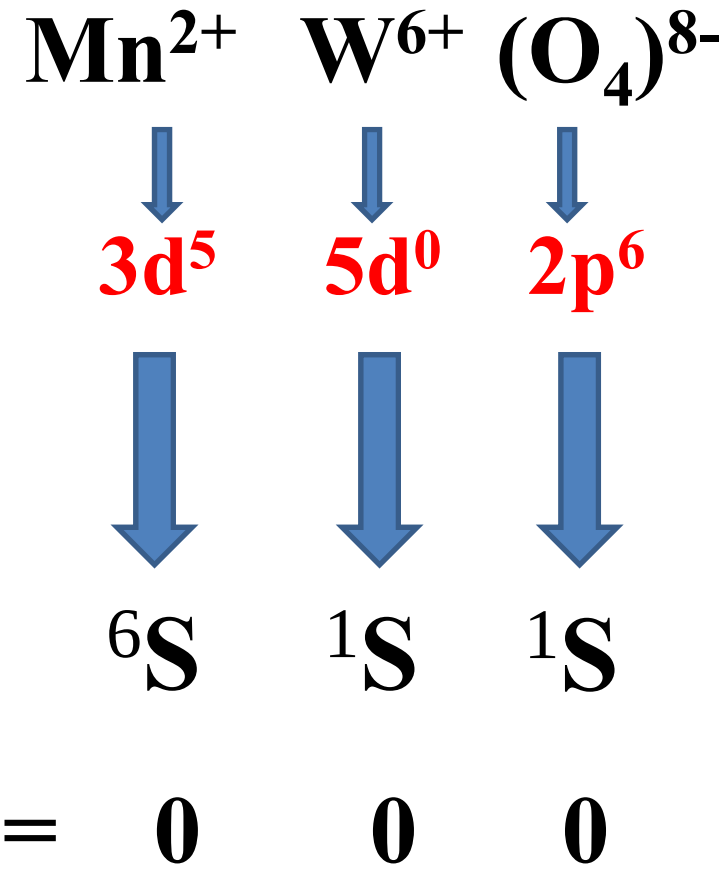

Motivation: Why is spin-orbit coupling important in an orbitally degenerate system?

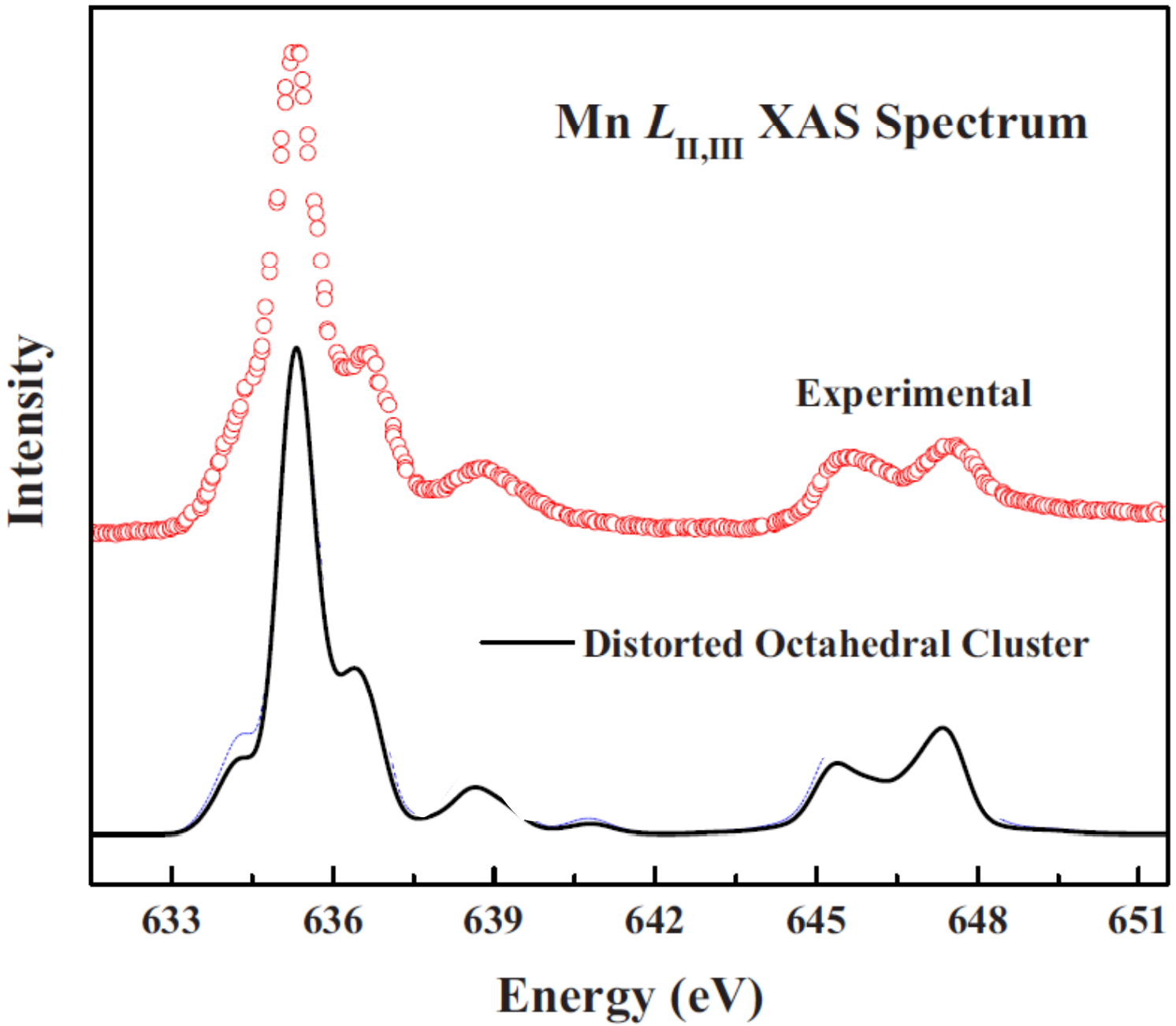
Mn $L_{II,III}$ XAS Spectrum
Experimental
Distorted Octahedral Cluster
Intensity
633
636
639
642
645
648
651
Energy (eV)

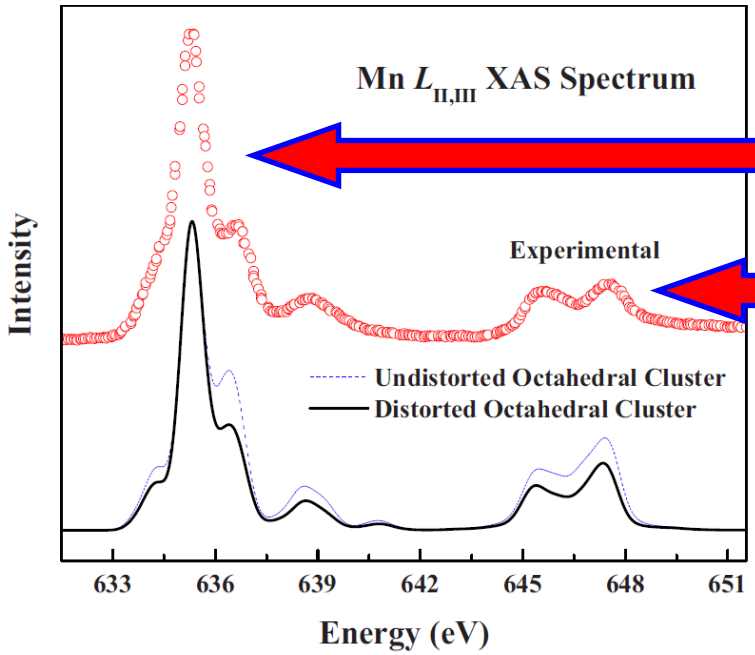

$2p^{10}\ 3d^{n} \rightarrow 2p^{9}\ 3d^{(n+1)}$

$2p^{9} \sim 2p_{3/2}$

$2p^{9} \sim 2p_{1/2}$

For the calculation, we consider:

$(MnO_6)^{10-}$ cluster

U_{dd} =4.0 eV, Δ =7.0 eV, $10Dq$ = 0.5 eV, and $pd\sigma = -1.29$ eV

3d occupancy, n_{3d}, of 5.14

86.5% d^5, 13% d^6L^{-1}, and 0.5% d^7L^{-2} characters

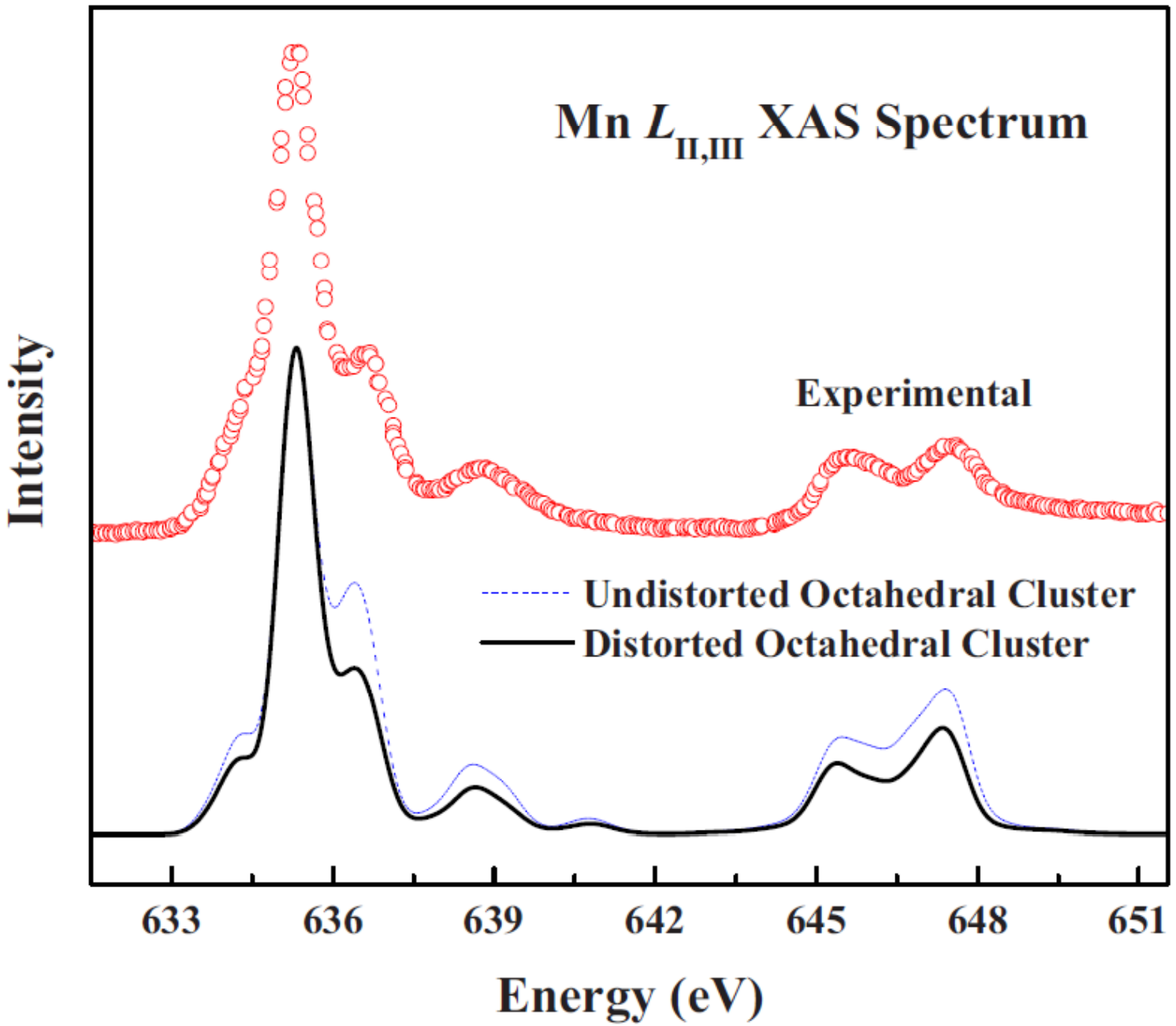
Mn $L_{II,III}$ XAS Spectrum
Experimental
Undistorted Octahedral Cluster
Distorted Octahedral Cluster
Intensity
633
636
639
642
645
648
651
Energy (eV)

Interface/intergrowth

Motivation: What happens with solidification of miscible liquids across an imiscible phase, particularly if one is a ferromagnet and the other a ferroelectric?

Percolative Conduction in the Half-Metallic-Ferromagnetic and Ferroelectric Mixture of (La,Lu,Sr)MnO_3

S. Park, N. Hur, S. Guha, and S.-W. Cheong, Phys. Rev. Lett. 92, 167206, 2004

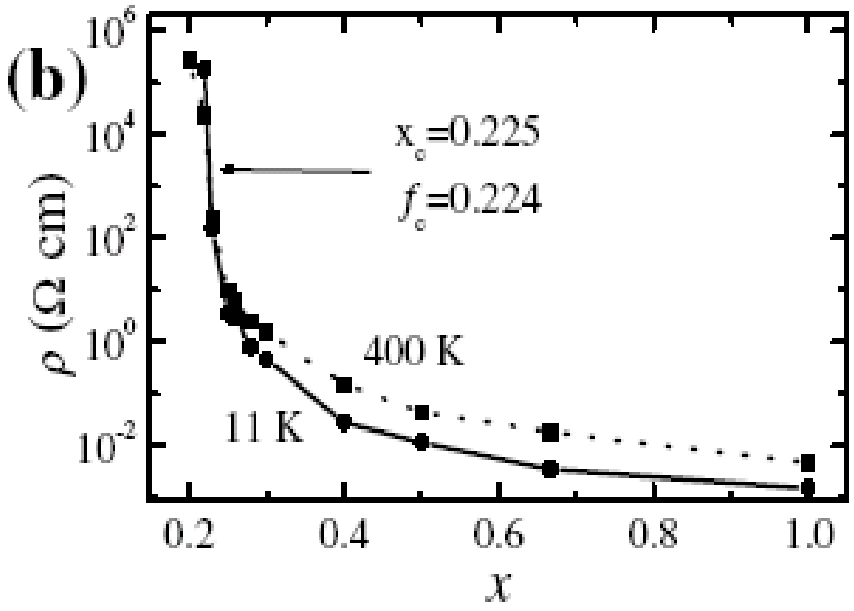

FIG. 3. (a) Resistivity of (x)LSMO:$(1-x)$LMO as a function of temperature for various metallic *molar* ratios, x. Dotted lines represent LSMO:$YMnO_3$. (b) Resistivity at 400 and 11 K as a function of x. f represents metallic *volume* ratios, and percolation threshold is chosen as $f_c = 0.224$, corresponding to $x_c = 0.225$.

The Spectromicroscopy Beamline at ELETTRA

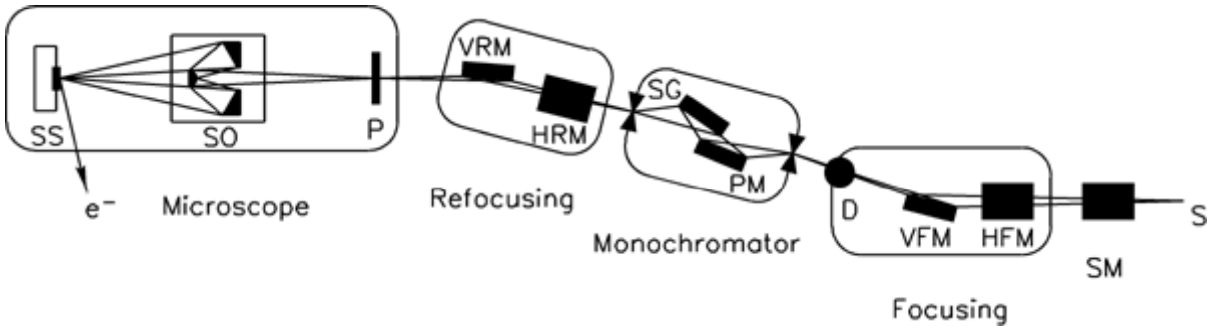

Available objectives: 20-25 eV
74 eV
95 eV ←
110 eV

Spatial resolution: 0.5 µm

Spectroscopic performances (e.g. on Au 5d):
3×10^5 cps with $\Delta E < 0.15$ eV

Best achievable energy resolution (aimed value):
30 meV

Recent upgrade:
coupling of scanning stage with cryostat
liquid N_2 operation since May 2001 (T ~ 90 K)
liquid He operation since October 2002 (T ~ 40 K)

ESCAmicroscopy layout

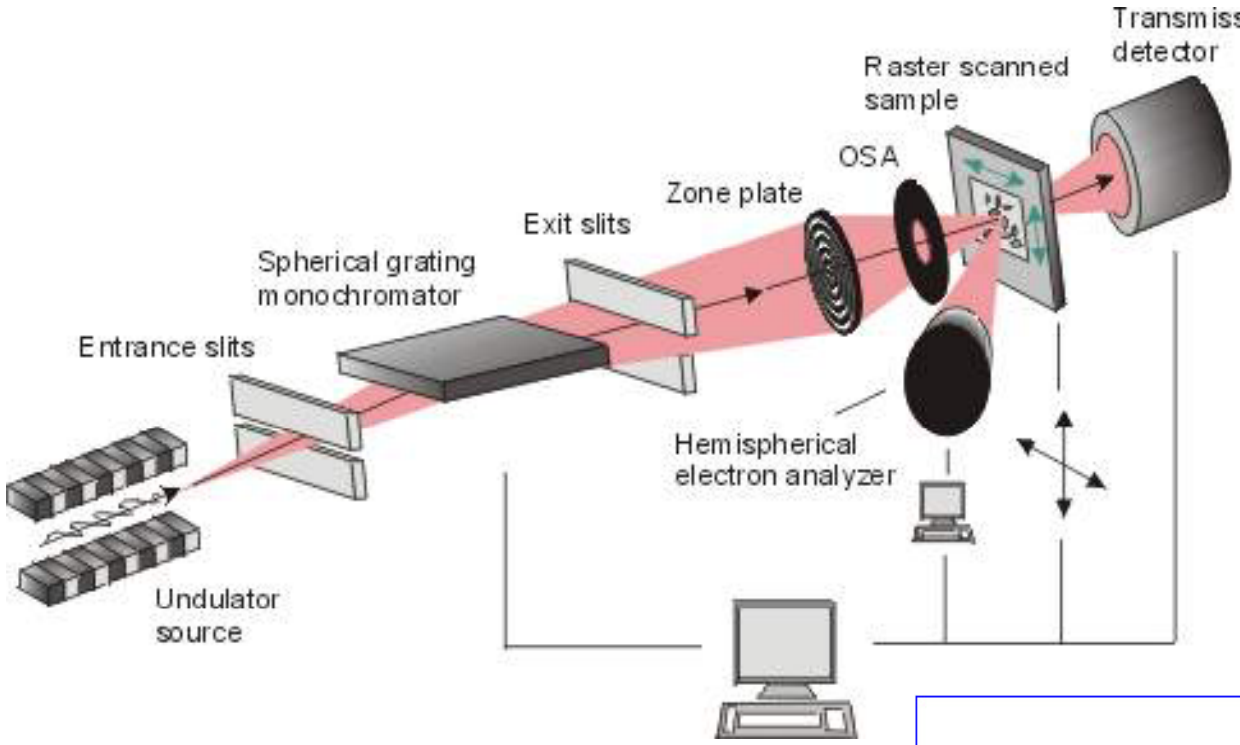

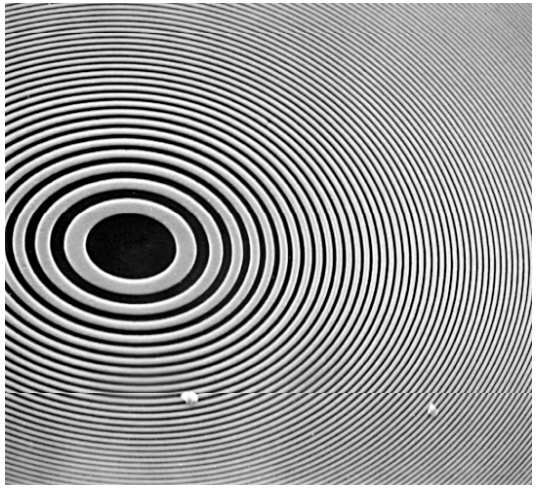

SEM image of the inner part of a Zone Plate

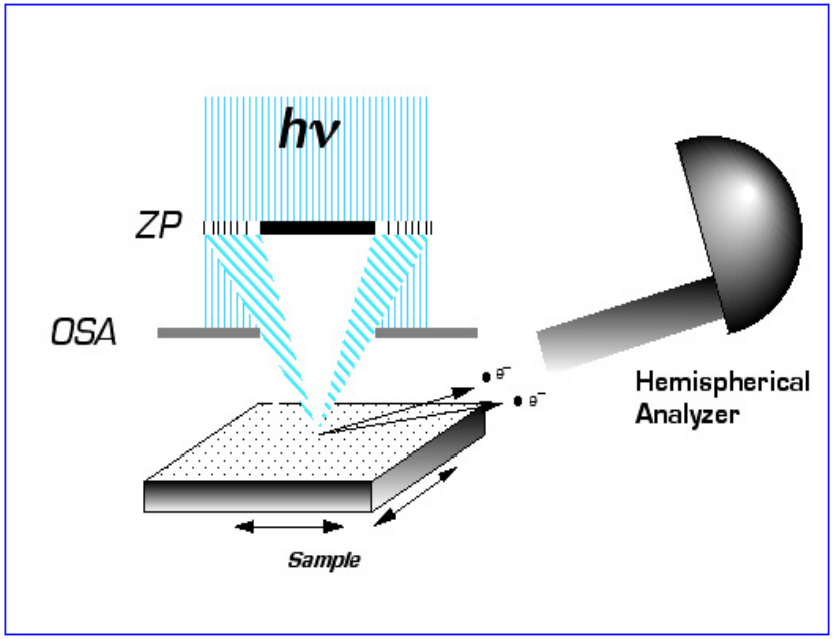

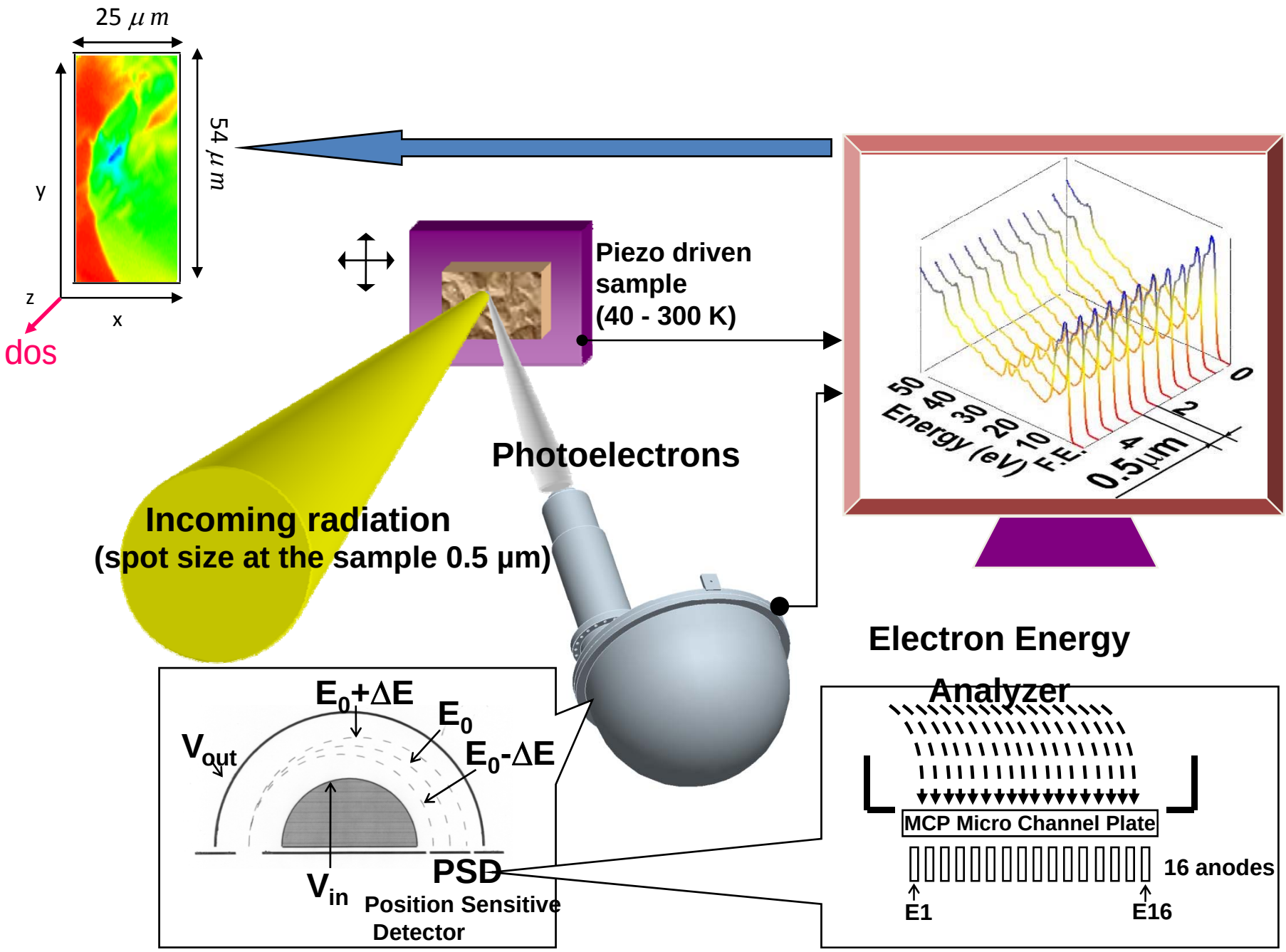
25 μm
54 μm
y
z
x
dos
Piezo driven
sample
(40 - 300 K)
Photoelectrons
Incoming radiation
(spot size at the sample 0.5 μm)
Energy (eV)
F.E.
0.5μm
Electron Energy
Analyzer
E0+ΔE
E0
E0-ΔE
Vout
Vin
PSD
Position Sensitive
Detector
MCP Micro Channel Plate
16 anodes
E1
E16

Experiment was performed at room temperature on "FZR-41" sample which is a combination of 0.79 $LuMnO_3$ + 0.21 $La_{5/8}Sr_{3/8}MnO_3$. A large number of spectra were collected at various points on the sample surface. We observed that most of the places in the sample are dominated by one type of spectra marked in red in figure 1, where as in some regions we got completely different spectra marked in black. On careful analysis we found that the spectra marked in red (which are abundant) are Lu rich as we see a strong signal of Lu 4f, while the spectra marked in black have larger La and Sr features (they also have larger intensity at the valence band, VB, near 3 eV binding energy). Therefore we have a phase separation, in terms of Lu rich grains and La and Sr rich grains.

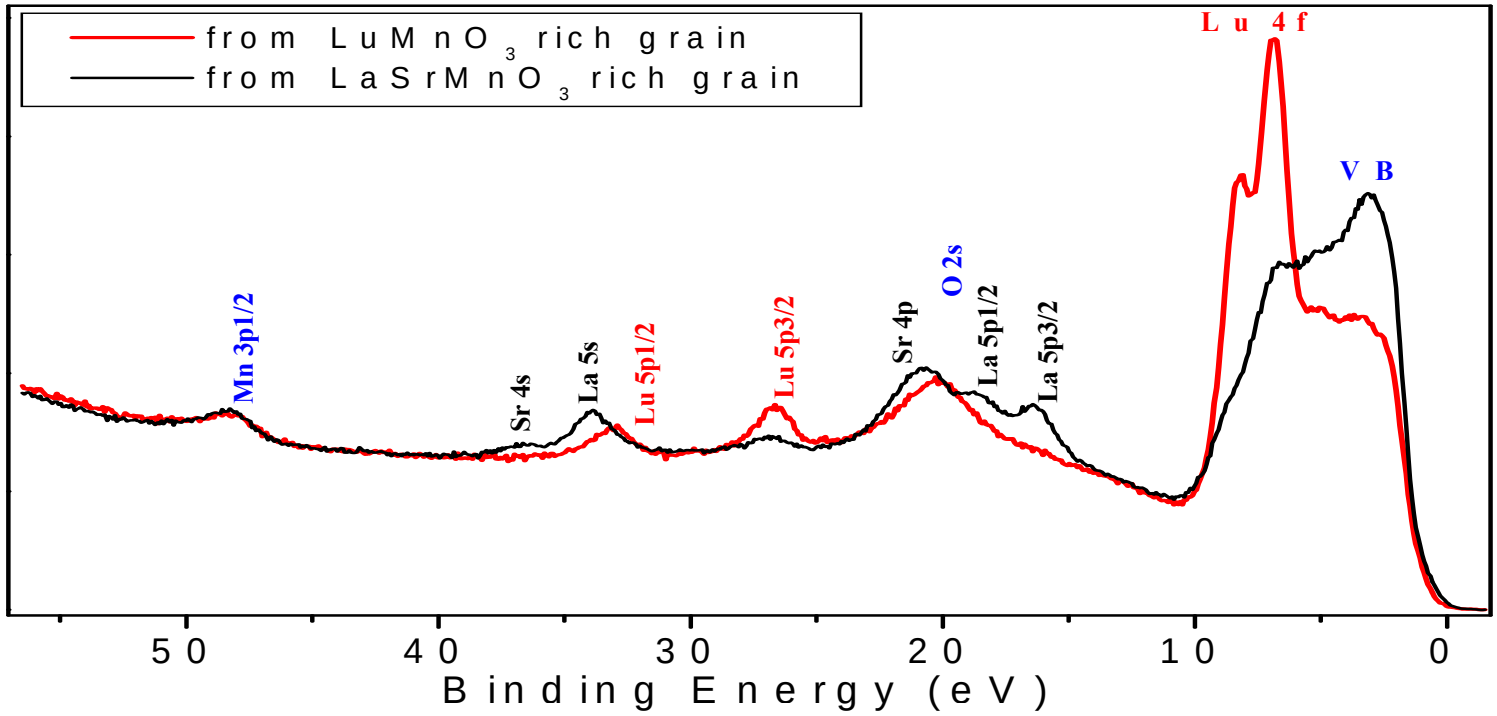

Fig1.

Spectra marked in red is from Lu rich grain, while that marked in black is from La and Sr rich grain. Texts are also given the similar color coding. Features which are common for both the grains are marked in Blue.

To find the length scale associated with the phase separation we collected a large number of intensity images at various places in the sample. The most striking difference in the two spectrum is at the VB and Lu 4f. though this is not the best place to look at the difference but due to the limitation of the energy window, which can cover only the features which are 7.2 eV wide in one image *(covering larger span in energy takes 20 times more time , we did this exercise also to do the final confirmation)* but as these differences correlate well with the two types of phases we utilized this difference in intensity to form the ratio images. Figure 2 shows a ratio image formed by dividing intensity collected by channels covering Lu 4f by the channels covering VB. Ratio image shows a strong contrast throughout the frame. We notice that most of the places in the frame are red in color and there are black stripes/patches in some places. We collected spectra at large number of black and red places in the figure and found that the spectra obtained from these two contrasting places are indeed different as shown in the figure 2 and discussed in figure 1. Hence the red region is basically $LuMnO_3$ and black region is $La_{5/8}Sr_{3/8}MnO_3$. It is interesting to note that there are two distinctly different length scales associated with the phase separation. There are large patches of $LuMnO_3$ which can be more than 70 µm in size while the stripes of $La_{5/8}Sr_{3/8}MnO_3$ are only 1-2 µm wide.

Fig 2.

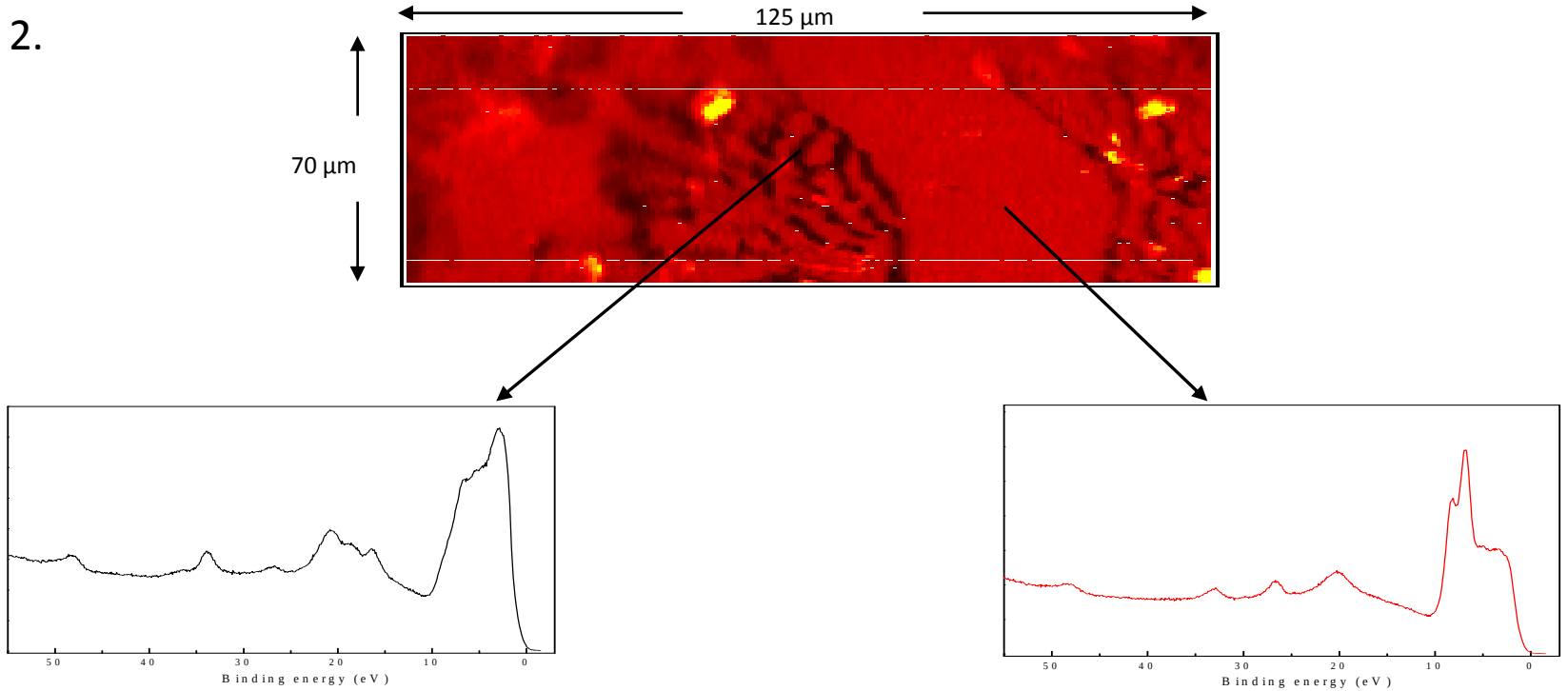

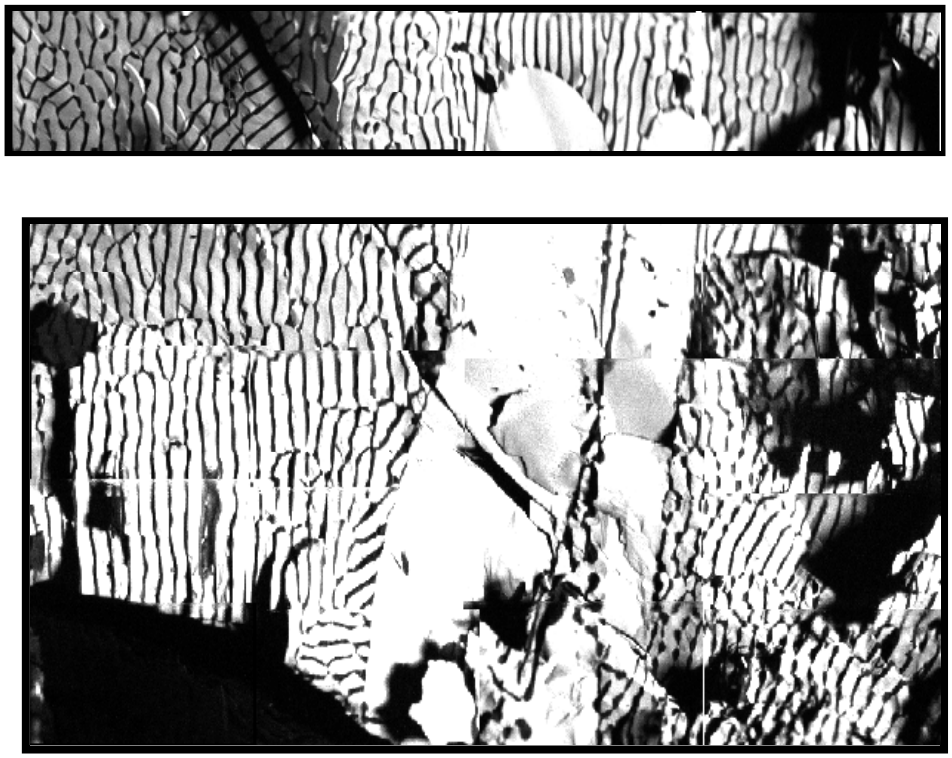

100 μm

200 μm

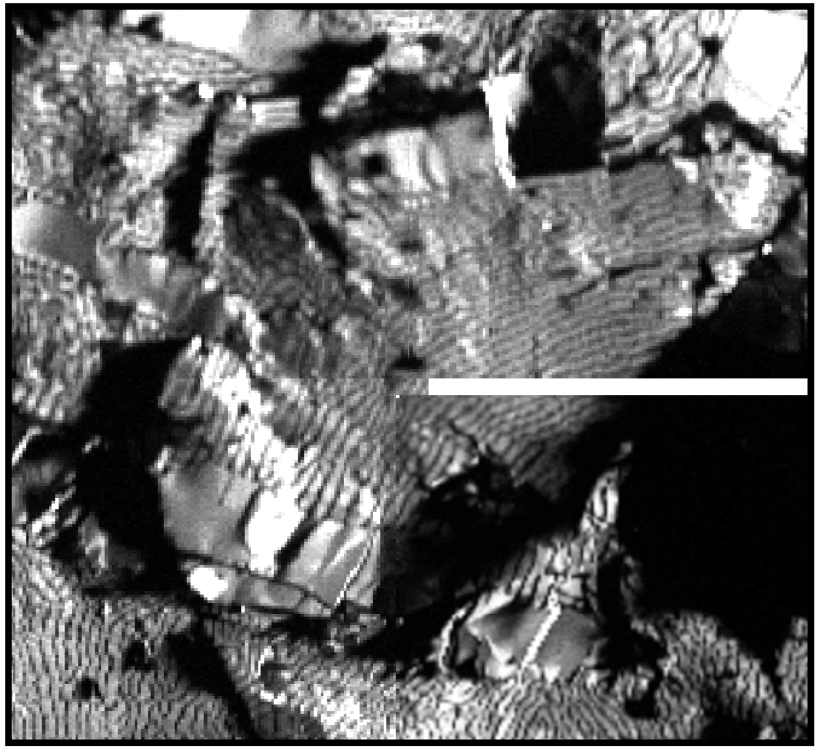

260 μm X 260 μm

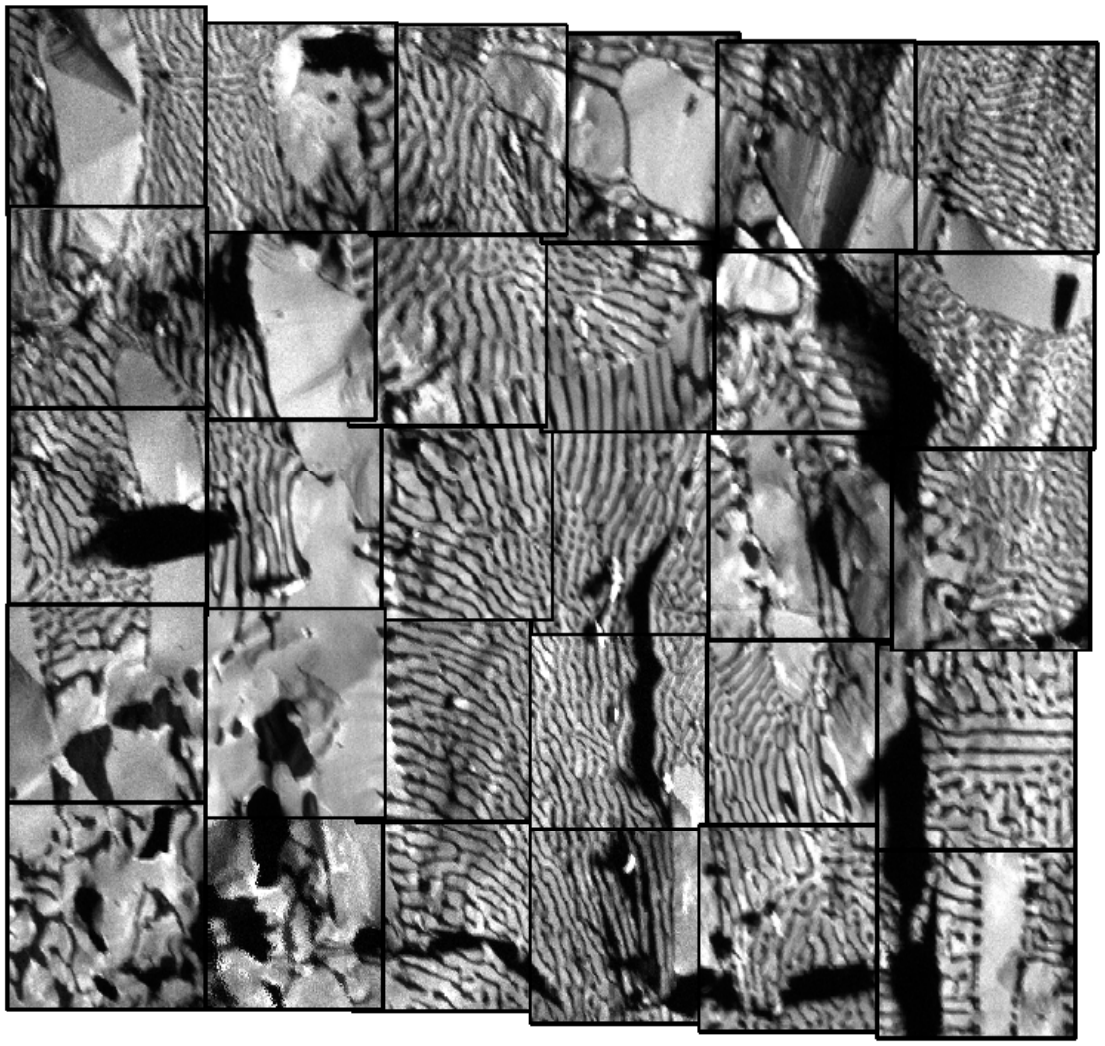

300 μm X 360 μm

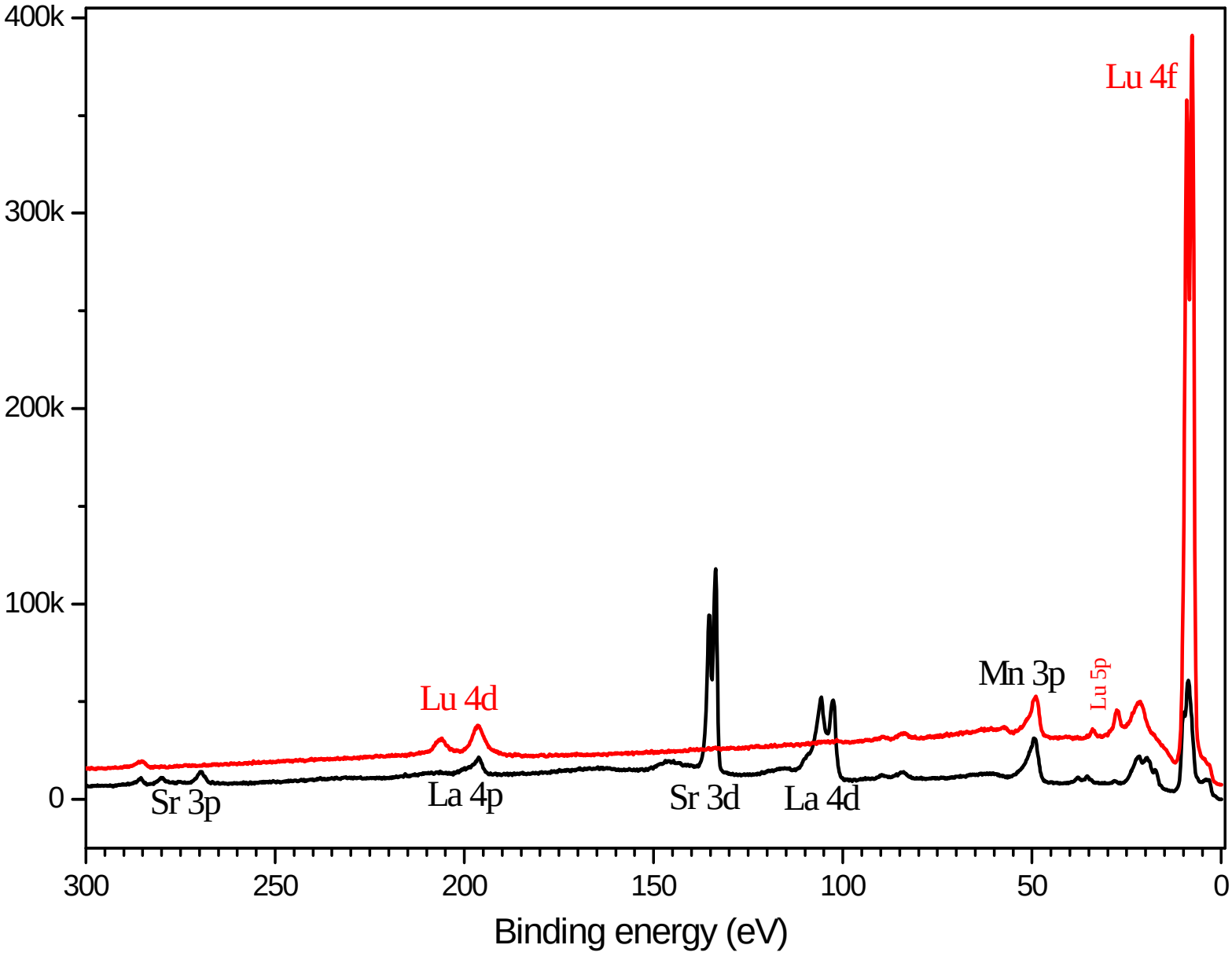
400k
300k
200k
100k
0
Lu 4f
Lu 4d
Mn 3p
Lu 5p
Sr 3p
La 4p
Sr 3d
La 4d
300
250
200
150
100
50
0
Binding energy (eV)

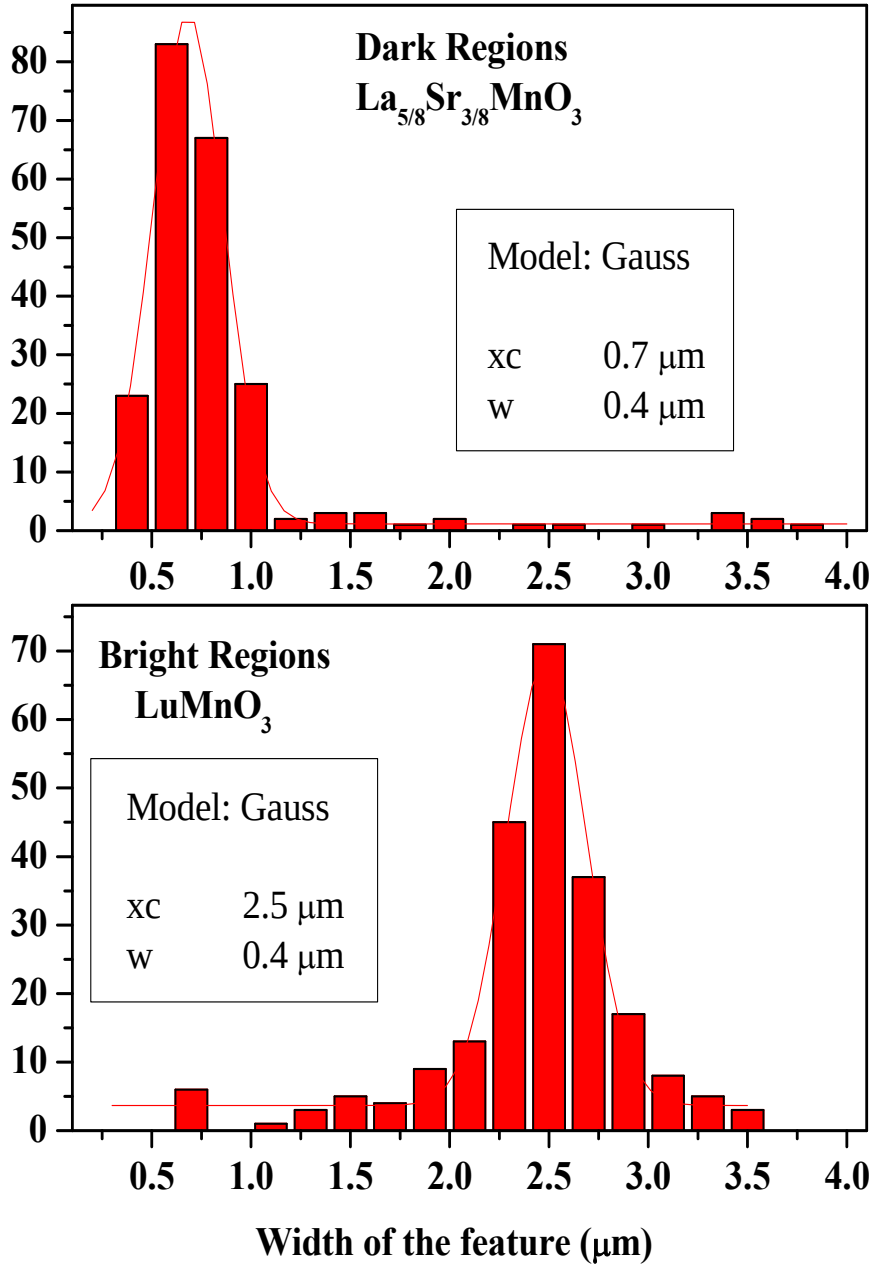

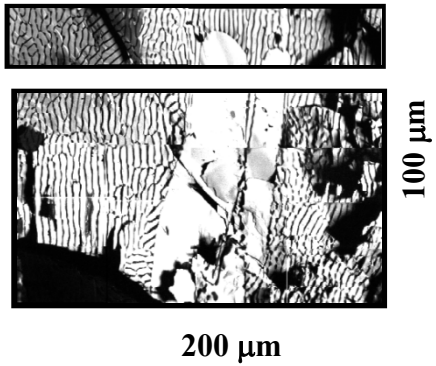

A very well-defined wavelength for the chemical phase separation.

ESCA-microscopy of $Eu_{0.5}Y_{0.5}MnO_3$ system, showing remarkable pattern formed by phase separation

Surajit Sengupta (SNBNCBS)
Gopal Shenoy; W.J. Liu (ANL)
John Budai, Jon Tischler, B. C. Larson (ORNL)
S.-W. Cheong (Rutgers)

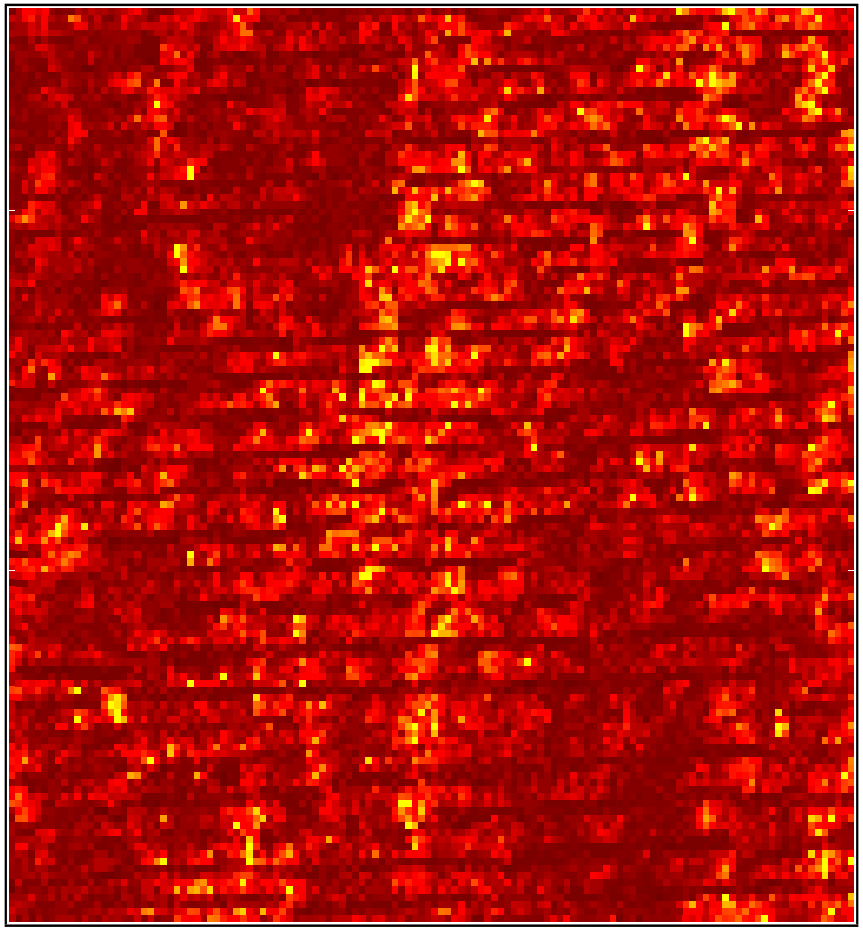

Spatially-resolved X-Ray Measurements - Depth Integrated

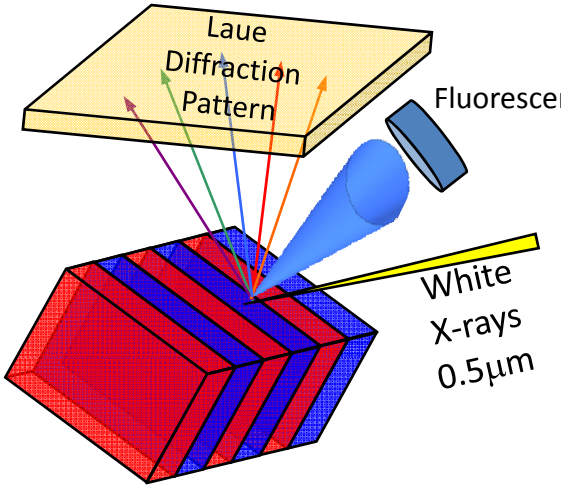

X-rays penetrate ~10-50 μm

Composition Maps from X-Ray Fluorescence

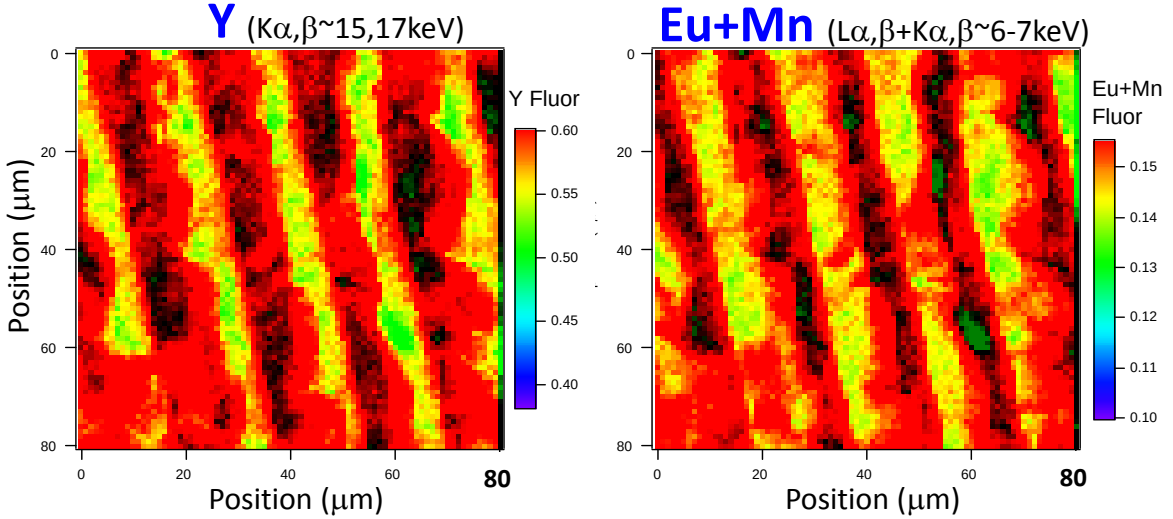

Structural (Phase) Information from X-Ray μ- Diffraction

Typical Laue (depth-integrated) = **Orthorhombic Phase** + **Hexagonal Phase**

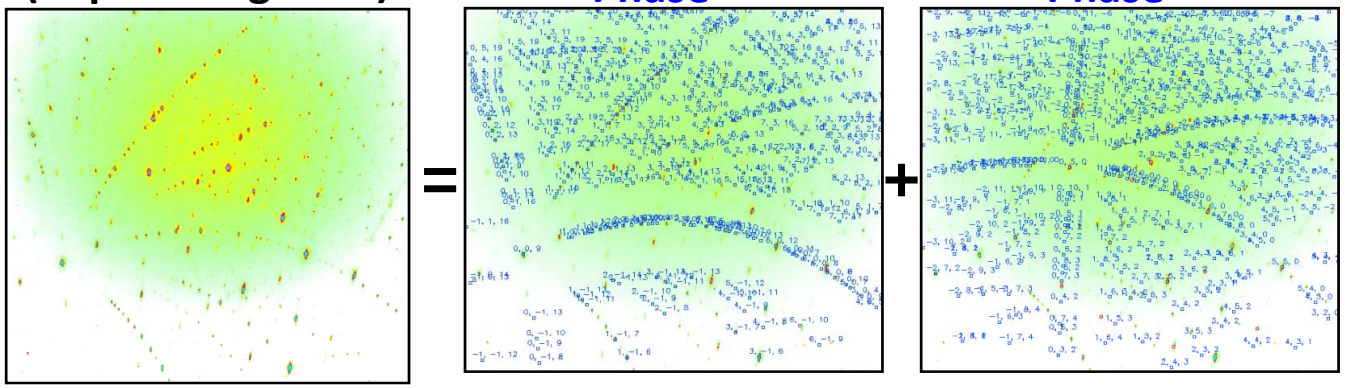

Every peak has a different energy.

Shape of pattern yields local lattice orientation and relative strain tensor

Adding monochromator (energy) yields absolute lattice parameter.

Intensities of Laue patterns ⇒ Spatial map of phases.

2D Structure Maps using mask analysis which sums intensities of particular Bragg peaks (indicated by the red rectangles and blue hexagons) from Laue patterns (no wire scans) for each phase. These are depth-integrated spatial maps of the ortho and hex phases. Clearly the ortho phase is spatially correlated with the Eu+Mn fluorescence and the hex phase is correlated with the Y fluorescence.

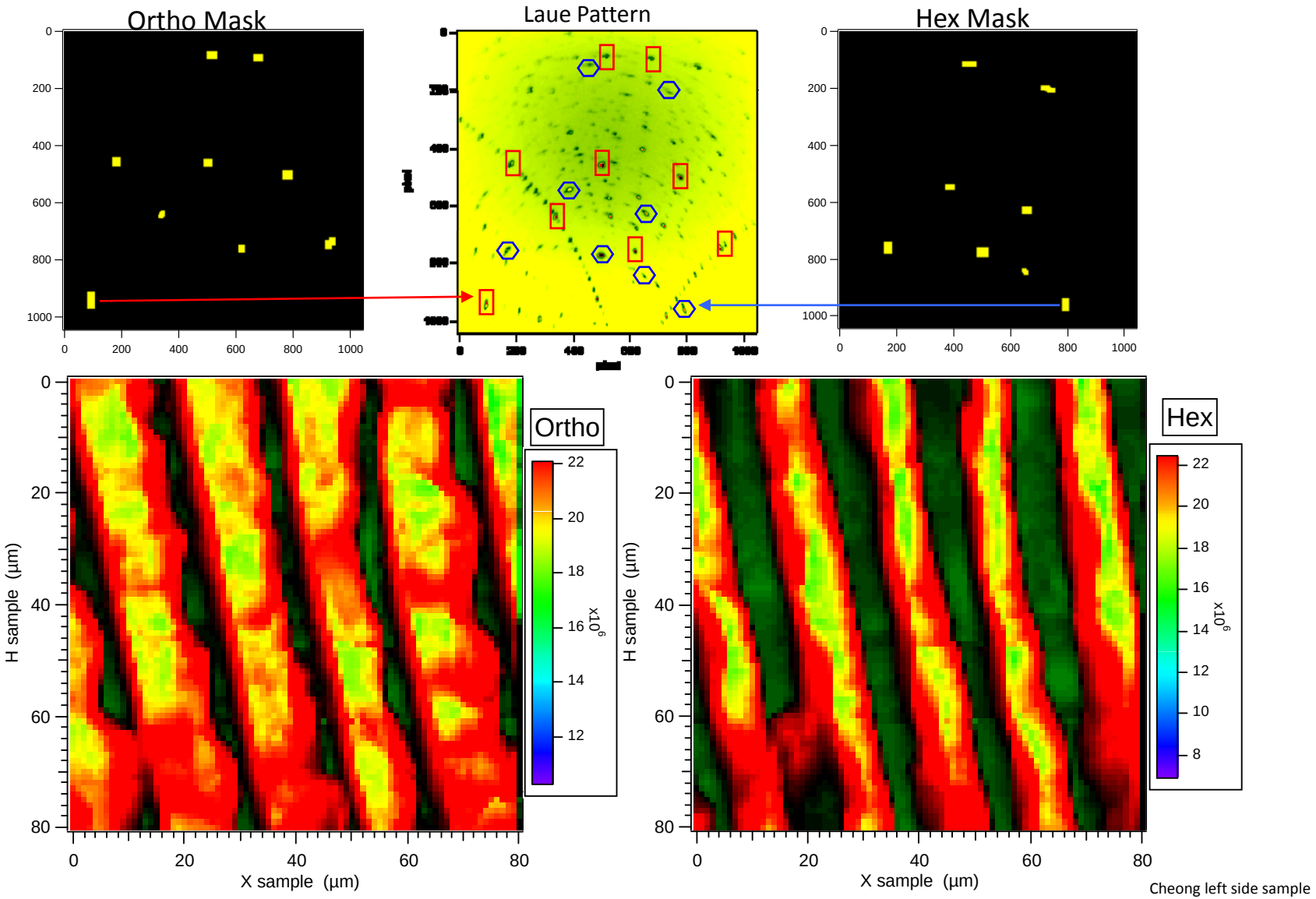

Construct Structural Maps from Intensities of Bragg Peaks for Each Phase.

These are **Depth-Integrated** maps with beam penetrating ~30μm

Laue Pattern

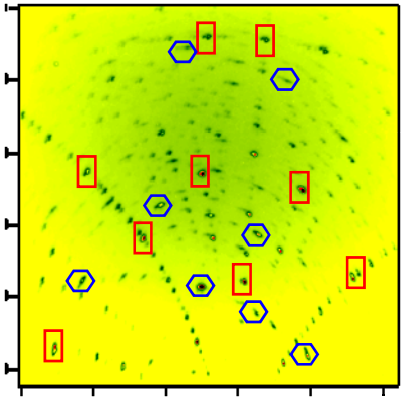

⇒

Hexagonal Phase

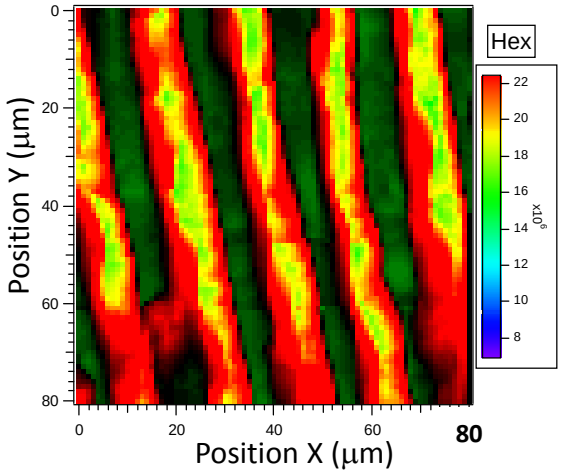

Orthorhombic Phase

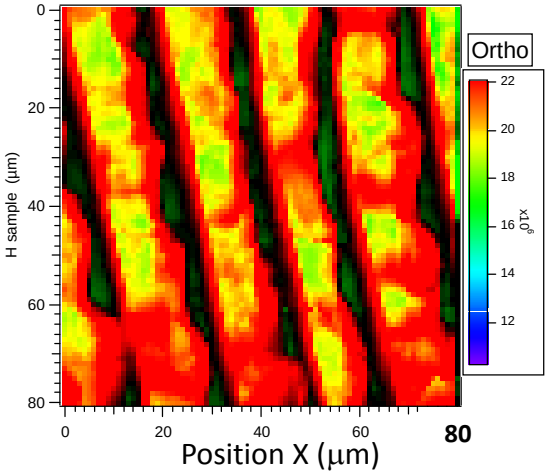

Combined Phase Map

Blue=Hex Red=Ortho

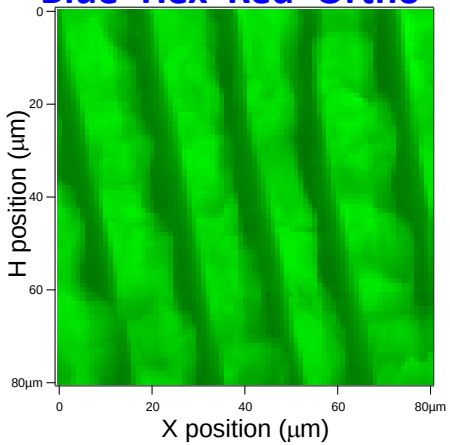

Y Fluorescence

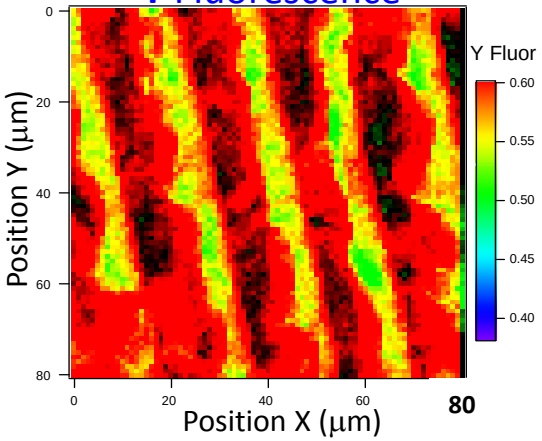

Eu+Mn Fluorescence

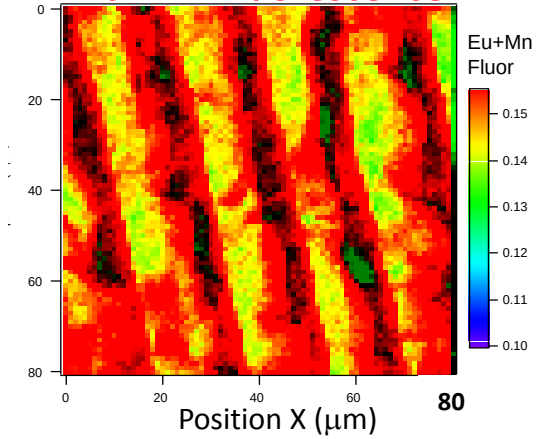

- Lamellar hex/ortho period ~15μm, Same as fluorescence, PES and optical.
- Hexagonal phase correlated with Y fluorescence; Orthorhombic phase with Eu fluorescence.
- Modulations along lamellae - Morphological growth instabilities will depend on kinetics of chemical diffusion and capillarity.

Measure Structure of Depth-Resolved Slice using Translating Wire

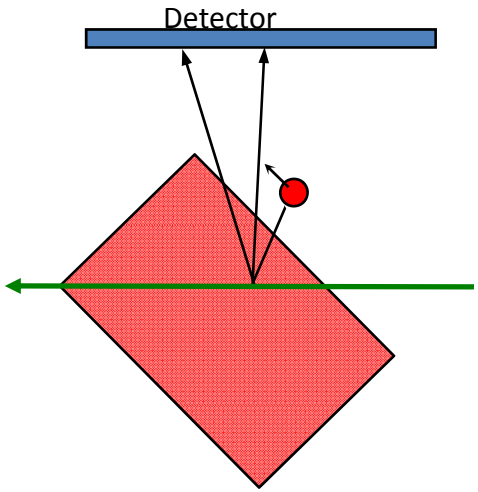

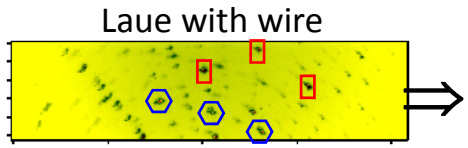

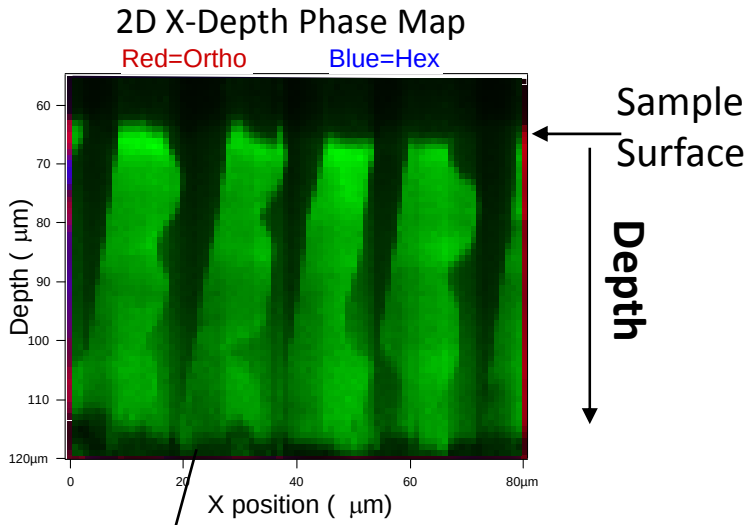

See Larson *et al*, Nature **415**, 887(2002)

Combine with previous depth-integrated scan of sample surface to obtain **3D phase map**.

The technique works! Each voxel contains **local** microstructure.

In principle, a full point-to-point 3D volume element can be measured using only depth-resolved scans.
Each 2D depth slice required ~8hrs due to slow detector readout.
Can increase >10x

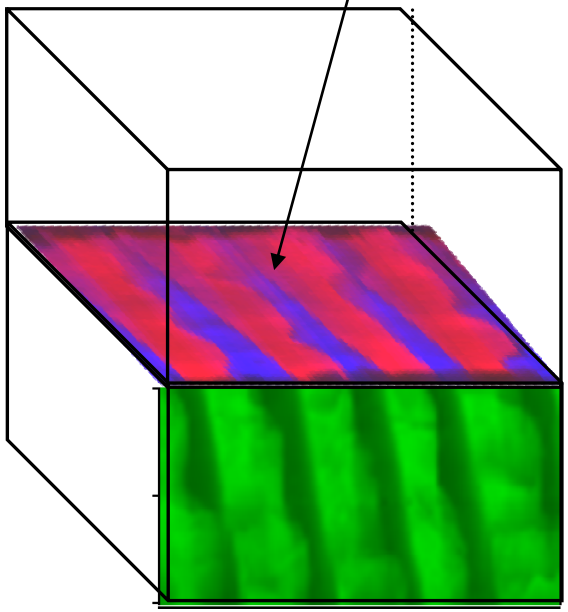

3D Spatially-Resolved Structure

Combine 2D White (depth-integrated) + 2D Depth-resolved (with wire) maps to try to show the 3D perspective in the same figure

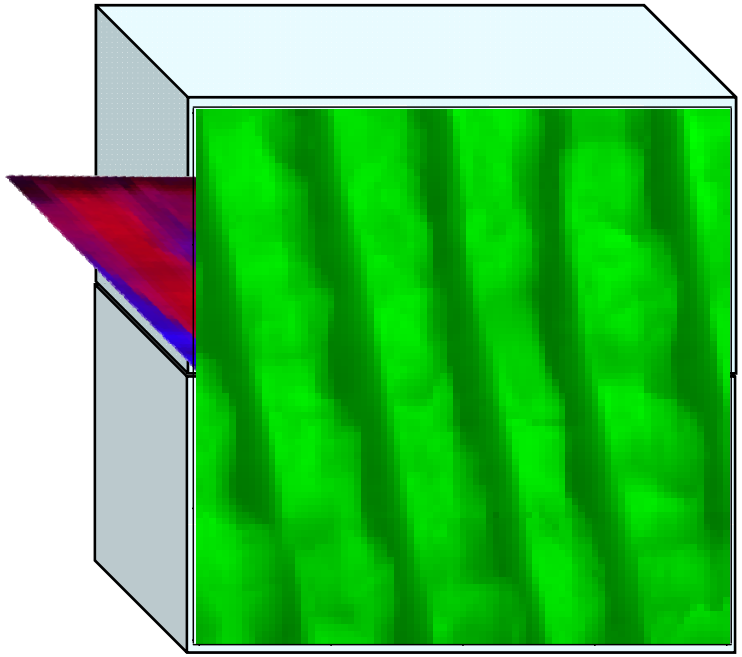

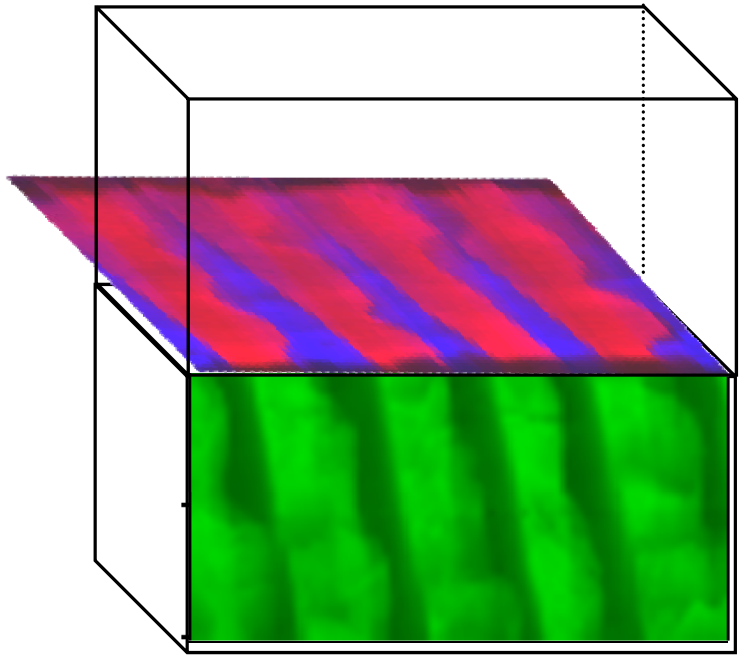

• $(La_{5/8}Sr_{3/8})_{0.21}Lu_{0.79}MnO_3$ phase separates in to nearly pure $(LaSr)MnO_3$ and $LuMnO_3$.

• EuYMnO breaks up in to two phases with approximately $Eu_{0.45}Y_{0.55}$ and $Eu_{0.55}Y_{0.45}$ compositions.

•The geometric pattern formed by the two phases suggest that it is probably driven by the presence of an eutectic composition in the vicinity of the sample composition.

Thank you for your attention